MAGNETIC MANIPULATION OF GRAVITATIONAL FORCE DURING CELL CULTURE

A Thesis Submitted to

the Graduate School of Engineering and Sciences of

İzmir Institute of Technology

in Partial Fulfillment of the Requirements for the Degree of

MASTER OF SCIENCE

in Bioengineering

by

Sinem KAPTAN

December 2022

İZMİR

ACKNOWLENGMENTS

I would like to express my deep and sincere gratitude to my supervisor Prof. Dr. Engin ÖZÇİVİCİ, for his guidance, support, encouragement, and patience throughout my research.

I am grateful to my esteemed committee members Assoc. Prof. Dr. Hüseyin Cumhur TEKİN and Assoc. Prof. Dr. Sinan GÜVEN. I am also grateful to Assoc. Prof. Dr. Gülistan MEŞE ÖZÇİVİCİ and Assoc. Prof. Dr. Özden YALÇIN ÖZUYSAL for her valuable support and guidance.

I would like to thank my best guiding Müge Anıl İnevi and Öykü SARIGİL for their support and help. I am also thankful to my teammates Melike ÇAĞAN, İlayda ÖZKAN, Melike KIZILKAYA, and Meltem GÜZELGÜLGEN for their support, and I would like to be grateful to Şüheda YAŞARBAŞ, Ece INAL and my dear friend Yağmur Ceren ÜNAL deserve special thanks for their help. I am thankful to my best friend in Izmir Elif BEYAZKAL for her motivation and encouragement in my difficult times and for the best 3 years we had. I also thank Seren KEÇİLİ for fabricating cell culture chamber.

I would like to gratefully acknowledge the support of The Scientific and Technological Research Council of Turkey. This study was supported by The Scientific and Technological Research Council of Turkey (TUBITAK) with a scholarship under 2210/C National MSc Scholarship Program in the Priority Fields in Science and Technology, Grant No: 1649B022102012.

The biggest thanks are for my beloved family. My mom Nuray KAPTAN, my father Nejdet KAPTAN, and my brother Sinan KAPTAN were always the biggest supporters in my life. I am very lucky to have a family that always believed in my dreams and supported me; every good thing and every success in my life is due to their efforts and their love for me, so I owe my dear family a debt of gratitude.

To my lovely family

To all the children who love space...

ABSTRACT

MAGNETIC MANIPULATION OF GRAVITATIONAL FORCE DURING CELL CULTURE

With the development of space technologies, one of the most important problems that astronauts will encounter in the planned manned space travels to the Moon and Mars in the near future is the reduced (<1g) gravitational force. Knowledge of the biological effects of partial gravitational force on long-duration space missions is limited. Therefore, it is important to investigate effects of partial gravitational force on physiological adaptation mechanisms. However, methodology to induce partial gravity is expensive and subjected to ethical constraints, therefore there is a need for new ground-based simulation platforms that are able to mimic the partial gravitational force. In this master's thesis, a new partial gravity platform was developed that manipulates gravitational force during cell culture using magnetic fields. First, the platform system was designed and fabricated, and then detailed protocols were described for its use in cell culture. In addition, the effect of simulated partial gravity on cell viability and morphology at the cellular level was examined. The results show that the simulated partial gravity of Mars and the Moon affects the viability and morphology of cells. This new low-cost and easy-to-use partial gravity platform can be used as a ground-based simulation system for gravitational space biology research at the cellular and molecular levels.

ÖZET

HÜCRE KÜLTÜRÜ SIRASINDA YERÇEKİMİ KUVVETİNİN MANYETİK MANİPÜLASYONU

Uzay teknolojilerinin gelişmesiyle birlikte yakın gelecekte Ay ve Mars'a planlanan insanlı uzay yolculuklarında astronotların karşılaşacakları en önemli sorunlardan biri azalan (<1g) yerçekimi kuvvetidir. Kısmi yerçekimi kuvvetinin uzun süreli uzay görevlerinde biyolojik etkileri hakkındaki bilgiler sınırlıdır. Bu nedenle, kısmi yerçekimi kuvvetinin fizyolojik adaptasyon mekanizmaları üzerindeki etkilerinin araştırılması önemlidir. Bununla birlikte, kısmi yerçekimini üretebilen metotlar pahalıdır ve etik kısıtlamalara tabidir, bu nedenle kısmi yerçekimi kuvvetini taklit edebilen yeni yer tabanlı simülasyon platformlarına gereksinim duyulmaktadır. Bu yüksek lisans tezinde, manyetik alan kullanılarak hücre kültürü sırasında yerçekimi kuvvetini manipüle edebilen yeni bir kısmi yerçekimi platformu geliştirilmiştir. Öncelikle platform sistemi tasarlandı ve üretildi daha sonra hücre kültüründe kullanımı için ayrıntılı protokoller tanımlanmıştır. Ayrıca, simüle edilmiş kısmi yerçekiminin hücre canlılığı ve morfolojisi üzerindeki etkisi hücresel düzeyde incelenmiştir. Sonuçlar, simüle edilen Mars ve Ay'ın yerçekimi kuvvetinin hücrelerin canlılığını ve morfolojisini etkilediğini göstermektedir. Bu yeni düşük maliyetli ve kullanımı kolay kısmi yerçekimi platformu, hücresel ve moleküler seviyelerde yerçekimi uzay biyolojisi araştırmaları için yer tabanlı bir simülasyon sistemi olarak kullanılabilme potansiyeli taşımaktadır.

TABLE OF CONTENTS

LIST OF FIGURES

Figure **Page**

Figure **Page**

Figure **Page**

Figure **Page**

CHAPTER 1

INTRODUCTION

1.1. Gravitational Biology

Gravity is an essential biomechanical signal affecting fundamental processes in the cells as life on Earth has evolved and developed under a constant gravitational force (1 g). Research in gravitational biology aims to understand how cells perceive the force of gravity and respond to it from the molecular level up to the organism [1,2]. Therefore, studies related to gravitational biology are necessary to understand the influence of gravitational force on cells in reduced-gravity environments such as microgravity and partial gravity [3–6].

One of the most significant problems in space missions is alterations in gravitational levels [7]. Astronauts and cosmonauts are exposed to microgravity on long-duration or short-duration space missions. Therefore, the effects of microgravity on the human physiology have investigated over the years. According to these studies, exposure to prolonged microgravity leads to several physiological problems, including cardiovascular deconditioning, atrophy of muscles, bone loss, immune dysregulation, and shifts in the body fluids [8–17]. One of the most prominent consequences is bone loss as microgravity causes 1-2% of bone mass in weight-bearing bones in one month [16,18,19]. Hence, bone loss become prominent as a crucial problem for prolonged space flights.

Space agencies have been planning to send a human-crewed spacecraft to the Moon in 2024 and then to Mars in the near future, and the exploration of Mars is planned to last at least three years [20,21]. However, there is little information about the effects of partial gravity on the human body as access to real partial gravity will be only experienced on the surfaces of the Moon and Mars. Therefore, understanding the effects of partial gravity is vital for the astronauts' health during the Moon and Mars missions. Due to limited access to the actual partial gravity environments, ground-based partial gravity platforms are required to investigate the impacts of partial gravity and countermeasure them.

1.2. Facilities for Gravitational Biology

Microgravity environment (weightlessness or μg) is near zero gravitational force. Real microgravity experiments are conducted at the low Earth orbit, such as in the international space station (ISS), satellites or space shuttles. However, due to limited access to space flight and high costs, many ground-based microgravity facilities have been developed to better understand the effects of microgravity. These are parabolic flights [22,23], drop tower [24], 2D-clinostats [25], random positioning machines [26], rotating wall vessel [27] and magnetic levitation [28–31]. In addition, partial gravity studies become great important for future long-term exoplanetary missions to the Lunar and Martian environments. Therefore, there are a few partial gravity simulation models, such as parabolic flights [32], random positioning incubator [33,34], and quadrupedal partial weight bearing (PWB) [35,36]. Moreover, partial gravity models for studying physiological changes in the human body, including vertical body weight support systems, lower body positive pressure treadmills, tilted body weight support systems, supine suspension systems, centrifugation, and head-up tilt are shown in figure [37–41]. These models are useful to study the physiological influences of partial gravity on the human body. However, here the platforms will be emphasized that allow studies of the cellular level, and especially those related to bone loss.

1.2.1. Partial Gravity Simulations Models

One of the conditions that induce partial gravity is parabolic flights. Parabolic flights are widely used to investigate the short-term biological effects of microgravity [42]. In addition, it is possible to generate the partial gravity levels of the Moon (0.16 g) and Mars (0.38 g). However, parabolic flights have some limitations, such as being expensive, having a short duration of ~24 and 33 seconds, respectively, for the Moon and Mars (Figure 1), and intermixing with hypergravity levels [32]. Therefore, parabolic flights are insufficient to investigate the impacts of prolonged partial gravity on the cells.

Quadrupedal partial weight bearing (PWB), as an analog of partial gravity, is used to investigate the physiological effects of partial gravity on the human body using animal models such as mice and rats [35,36,43–45]. This analog allows studying partial gravity effects

at tissue and organism levels. However, it is not suitable for investigations at the cellular level.

Random Positioning Machine (RPM^{SW}) platform and developed random positioning incubator from RPM enables to simulate about partial gravity of the Moon or Mars [33,46]. RPM can be used to investigate effects of partial gravity at the cellular or molecular levels. However, random position machine has disadvantage that can lead to shear stress on cells that due to fast rotation and a deformation of the cell membrane, inducing an unintended and unrealistic mechanical loading on cells and confounding results [47,48].

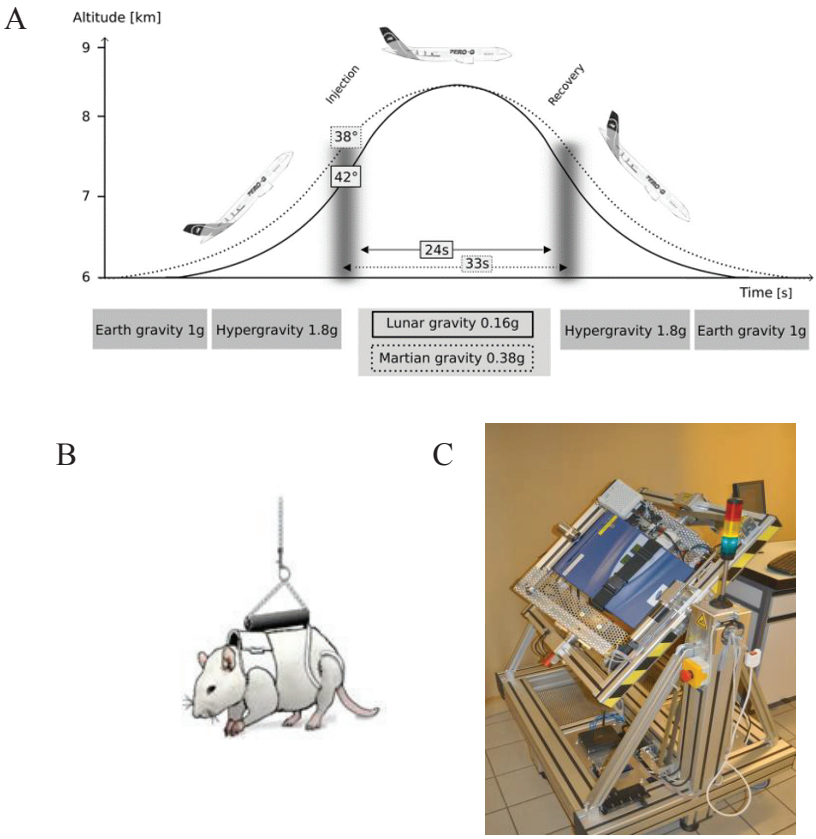

Figure 1. Partial gravity simulation models A) Parabolic flights [49], B) Quadrupedal partial weight -bearing [35], and C) Random positioning machine [33].

1.3. Biology of Bone Tissue

Bone is a consistently renewed dynamic tissue and contains four types of cells: bone lining cells, osteoblasts, osteocytes, and osteoclasts [50,51]. New bone is formed by osteoblasts while old bone is removed by osteoclasts (Figure 2). There is a balance between bone formation and resorption of bone. This balance may be impaired due to osteoporosis or exposure to microgravity [52–56]. Osteoporosis is associated with decreased bone mass and deterioration of the microarchitecture of the bone, which increases the risk of fracture [53]. Exposure to microgravity results in bone loss by disturbing the bone remodeling process [57]. Consequently, osteoblasts are responsible for bone formation and play a vital role in the maintenance of bone health.

Osteoblasts are specialized fibroblast cells derived from mesenchymal stem cells. They produce organic and inorganic constituents of the bone extracellular matrix, such as type I collagen, osteocalcin, osteopontin, and calcium-phosphate-hydroxide salt called hydroxyapatite as an inorganic mineral [58]. Mesenchymal stem cells differentiation into osteoblast occurs in three steps: cell proliferation, matrix maturation, and matrix mineralization. The matrix mineralization is the final step for osteogenic differentiation and can be detected by calcium deposits [59]. Osteogenic differentiation is determined by the unique molecular-based osteogenic markers, such as alkaline phosphatase (ALP), collagen I, and Runx2 or by imaging of calcium deposits by Alizarin Red or von Kossa staining [59].

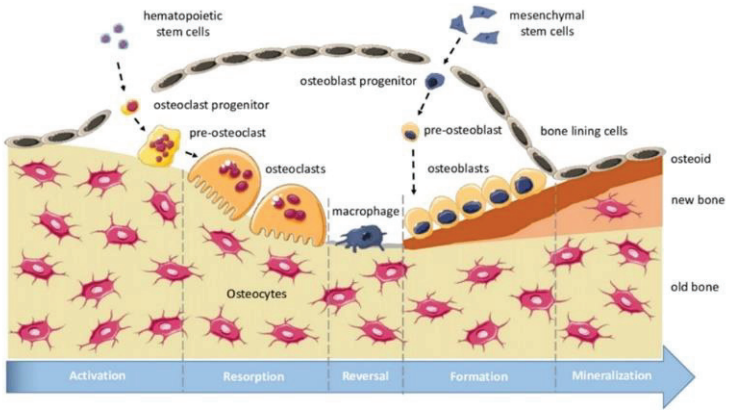

Figure 2. Bone tissue cells consists of bone lining cells, osteoblasts, osteocytes, and osteoclasts. New bone is formed by osteoblast and old bone is removed by osteoclasts [60].

1.3.1. Effects of Reduced Gravity on Osteoblasts

Gravitational force is perceived by cells as a mechanical signal, and most cells respond to changes in gravitational force, such as microgravity and partial gravity. The effects of microgravity on bone cells have been extensively investigated in in-vitro and in-vivo, especially osteoblasts. Osteoblasts are one of the gravity-responds cells [61,62]. Microgravity leads to a decreased in proliferation of the osteoblasts and osteogenic differentiation of the mesenchymal stem cells, whereas an increase in adipogenesis also microgravity induces osteoclastogenesis [63–65]. Therefore, reduced gravity leads to bone loss by inhibiting the growth, proliferation, and differentiation of osteoblasts. On the other hand, exposure to partial gravity causes a dose-dependent reduction in proliferation and the enzymatic activity of alkaline phosphatase in osteoblasts [66]. Also, cellular morphology is affected by changes in mechanical loading. The cytoskeleton plays a role in the morphology of the cells. Changes in the function of the cytoskeleton induce as a response to alterations in gravitational force [67]. Altered gravity results in changes in the actin filaments of osteoblasts [68]. Taken together, osteoblasts may be sensitive to changes in gravitational force.

1.4. Magnetism of Objects

Magnetic flux density or magnetic induction B (Tesla or T) defines the number of field lines passing through a unit area of the medium as a response to an applied external magnetic field. Magnetic permeability is an intrinsic property of materials and is associated with the density of magnetic field lines [69]. Magnetic susceptibility (χ) is the degree of magnetization of material and allows classifying materials as diamagnetic, paramagnetic, and ferromagnetic based on magnetic behavior [70,71]. Diamagnetic objects ($\chi < 0$, $\sim -10^{-6}$ - -10^{-3}) do not have a net magnetic dipole moment without applying an external magnetic field. However, when an external magnetic field is applied, the dipole moment is directed opposite the external magnetic field. As a result, the material is repelled by the external field. Water, proteins, and cells are examples of diamagnetic objects. Paramagnetic objects ($\chi > 0$, $\sim 10^{-6}$ - 10^{-1}) have dipole moments formed along

the direction of an external magnetic field such as oxygen, aluminum, and gadolinium. Ferromagnetic objects ($\chi >> 0$) exhibit parallel alignment of moments even when the external magnetic field is removed, such as iron, cobalt, and nickel [72,73]. Neodymium magnets are permanent magnets, and ferromagnetism is used to induce permanent magnets. Neodymium magnets are composed of neodymium, iron, boron, and a few transition metals (Nd-Fe-B) as well as there are different grades of neodymium magnets from N35 to N52. Among them, N52 has the highest magnetic performance [74].

1.4.1. Magnetic Liquids

Paramagnetic solutions are used as a contrast agent in diagnostic magnetic resonance imaging (MRI) such as gadolinium-based contrast agents and widely used to enhance the contrast of images of organs and tissue of the body. GBCAs can be classified into two major groups: linear and macrocyclic. The linear type is open chain molecules, whereas macrocyclic Gd^{3+} is caged by an organic ligand [75]. Free Gd^{3+} is toxic because of the similar size radius with Ca, allowing Gd^{3+} to compete biologically with Ca^{2+} in calcium- dependent channels [76]. The macrocyclic agents are more stable than linear types [77]. Gadobutrol is a non-ionic, macrocyclic agent that is chelated with butrol (Figure 3). Gadobutrol (Gadovist/Gadavist) has high biocompatibility and based on this feature, is used in magnetic manipulation of living cells [78–82].

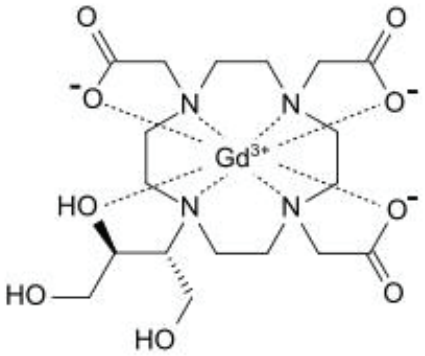

Figure 3. Molecular structure of gadolinium contrast agent, Gadavist (Source: Trog et. al.,2019) [83].

1.5. Halbach Array

A Halbach array is a special arrangement of permanent magnets in which the magnetic field on one side of the array is strong while the magnetic field on the other side is weak. The Halbach array can be constructed linear or cylindrical (Figure 4) [84,85]. Halbach array has advantages and disadvantages. The major disadvantage of the Halbach array is holding together as the magnets repel each other. However, this drawback can be solved by using a strong adhesive. The advantages of the Halbach array are that it provides a strong and uniform magnetic field on one side of the array and easy-to-make as well as, cost-effective [86]. In addition, The Halbach array is capable of being used to separate cells and particles [87–89].

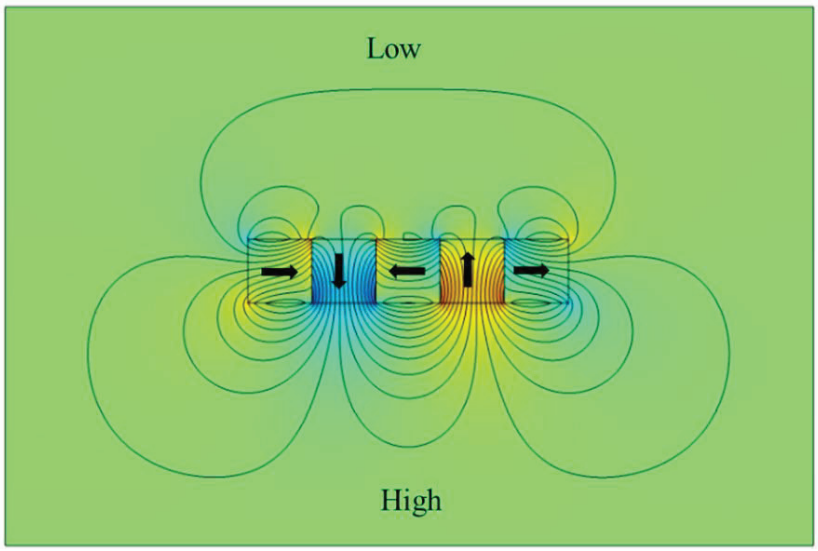

Figure 4. Halbach array configuration type of linear.

1.6. Aim of the study

One of the fundamental forces is gravitational force and it has a magnitude and unidirectional. The gravity is denoted by g, while gravitational acceleration is expressed as m/s^2 and is equal to $N \cdot kg^{-1}$. The gravity on Earth is equal to 1 g, and gravitational acceleration is 9.81 m/s^2. However, Mars and the Moon have a reduced gravity than Earth. The gravity of the surface of Mars 3.7 g (3.7 m/s^2) and the Moon is 1.6 g (1.6 m/s^2). Gravitational force cannot be canceled on Earth, but it may be manipulated benefits from its direction or magnitude. Random positioning machines take advantage of the direction of gravity by spinning faster than the time of sensing gravity to simulate microgravity, while magnetic levitation is used magnetic force to compensate for the gravitational force. Gravitational acceleration is likely to be manipulate using a magnetic force by a Halbach array that has a strong and uniform magnetic field.

In this study, we aimed to present a new partial gravity simulation platform using the Halbach array. This platform allowed a unique opportunity to investigate the consequences of lunar and Martian fractional gravity at the cellular level. Therefore, this platform could be used as a ground-based partial gravity simulation model due to its low-cost, easy-to-use, and to allow cellular studies at short-and long durations.

CHAPTER 2

MATERIALS AND METHODS

2.1. Principle of Magnetic Force

A magnetic dipole is formed to the opposite direction the magnetic field when an external magnetic field is applied to diamagnetic objects such as cells. Therefore, the cells tend to move towards a lower magnetic field region in a paramagnetic medium. In our system, the dominant forces on the cells are magnetic force and gravitational force. F_{mag} is a magnetic force, where V is cell volume, χ_m is magnetic susceptibility of paramagnetic liquid, and χ_c is magnetic susceptibility of cells, μ0 is the permeability of free space (1.2566×10^{-6} kg·m·A^{-2}·s^{-2}), B is magnetic induction (Tesla, T) and ∇ is del operator (Eq. 1). F_g is gravitational force, where V is cell volume, Δρ is the density difference between cell and paramagnetic liquid, g is the gravitational acceleration (9.81 m/s^2) (Eq. 2). In our study, the magnetic force was used to reduce gravitational acceleration.

$$\vec{F}_M = \frac{V \cdot (X_c - X_m)}{\mu_0} (\vec{B} \cdot \nabla)\vec{B} \quad (1)$$

$$\vec{F}_g = v \cdot \Delta p \cdot g \quad (2)$$

2.2. Manipulation of Gravitational Acceleration

One of the fundamental forces is the gravitational force, which has a magnitude and vector. The gravity is denoted by g, while gravitational acceleration is expressed as m/s^2 and is equal to $N \cdot kg^{-1}$. The gravitational acceleration on Earth is equivalent to 9.81 m/s^2 (~1 g). Gravitational force cannot be canceled on Earth, but it may be manipulated by benefits from its direction or magnitude, hence in this study, when the magnetic force is less than the gravitational force ($F_g > F_{mag}$), the cells are not levitation at certain magnetic susceptibility of the paramagnetic liquid. That magnetic susceptibility values are crucial for this study. In the system, the density of cells, magnetic susceptibility of the medium, and the distance of the cell culture chamber from the magnets play an active role in mimicking reduced gravitational acceleration. In the acceleration equation, $(\vec{B} \cdot \nabla)\vec{B}$ is magnetic induction, $\Delta\chi$: magnetic susceptibility difference between the paramagnetic medium and the cell, $\Delta\rho$ is the density difference between the paramagnetic medium and the cell, g is gravitational acceleration (9.81 m/s^2) (Eq. 3). According to the gravitational acceleration equation, the acceleration value on cells is able to decrease from 9.81m/s^2 of the Earth to partial gravity levels. However, initially, mimicking the partial gravity of the Moon (1.6 m/s^2) and Mars (3.7 m/s^2) required paramagnetic medium concentration (Gd^{3+}) should be predicted.

$$a = \frac{\left(\frac{\left((\vec{B} \cdot \nabla)\vec{B}\right)}{\mu_0} \cdot \Delta_x + \Delta p \cdot g\right)}{\Delta p} \tag{3}$$

In order to reduce the gravitational acceleration on the cells, the positions of cells were arranged in a distance for corresponding paramagnetic Gd^{3+} concentrations in which there is a lower magnetic force than the gravitational force. However, it is difficult to determine needed Gd^{3+} concentrations for partial gravity one by one calculation. Therefore, multiple regression analysis was used to predict what concentrations of Gd^{3+} would be specifically required to simulate partial gravity.

2.3. Cell Culture Chamber Design Based on Selected Simulations

To simulate the fractional gravity of Mars and the Moon, the gravitational range was determined as ±10% of the 3.7 m/s^2 for Mars and 1.6 m/s^2 for the Moon. For this purpose, the diameters of the culture wells were determined as 3 mm for Mars and 2.4 mm for the Moon according to the selected simulation results.

2.4. Construction of Partial Gravity Cell Culture Chamber

The partial gravity cell culture chamber was designed according to the simulation results that showed the intended reduced gravitational acceleration range of 84% for the Moon and 62% for Mars. For this purpose, firstly, the desired chamber was drawn in LaserBox software to have five wells, and this chamber (PMMA) and double-sided tape were cut by a laser cutter (Makeblock LaserBox). The culture surface was selected as the cover glass, and before bond, the cover glass (0.15 mm thickness) was cleaned in an ultrasonic cleaner with 70% alcohol at 60 °C for 15 minutes. Finally, the plexiglass (PMMA) and the cover glass were bonded with double-sided adhesive tape, and for better bonding of the culture chamber, they were kept in the oven at 60 °C for 24 hours (Figure 5).

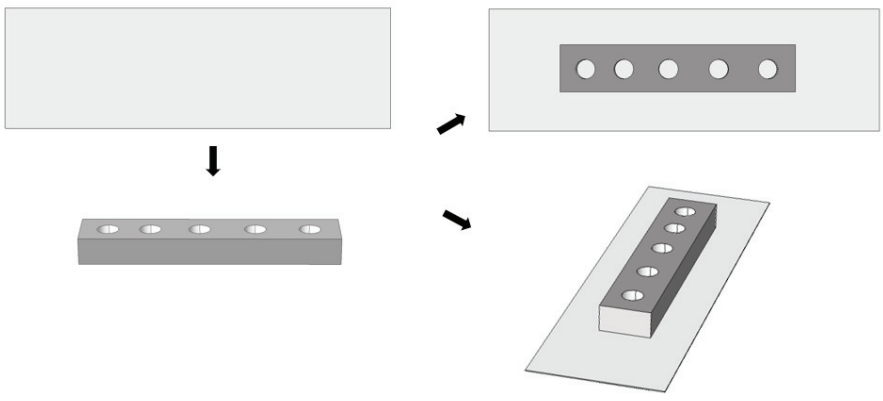

Figure 5. Production of the partial gravity cell culture chamber that is constructed with a coverslip and a PMMA by bonding with double-sided adhesive tape.

2.4.1. Construction of the Halbach Array

Our Halbach array design was composed of five neodymium magnets with dimensions 3/8" x 3/8" x 3/8" thick, purchased B666-N52 neodymium magnet by K&J. To construct the Halbach array, initially, the north pole of magnets was marked with a waterproof felt pen using a bar magnet, and they were taken on pieces of an iron plaque with 15x10 cm. The magnets were ranged to face the north pole by rotating 90°counterclockwise (Figure 6). A small piece of adhesive tape was put on each magnet to avoid confusing the magnets' directions, and the other iron plaque was put on the magnets. The glue was put between two magnets to stick the magnets and was pushed together sideways without space between the magnets. Finally, at least 12 hours should be waited to dry it.

Figure 6. Configuration of the magnets for the Halbach array.

2.4.2. Design of Holder Component for Halbach array

To better held the magnets, a holder component without one surface was designed for this specific Halbach array size (13.525 x 57.625 x 19.524 mm; height, length, and width), and the desired holder component was printed by a 3D printer (Ultimaker 2+ Connect) (Figure 7).

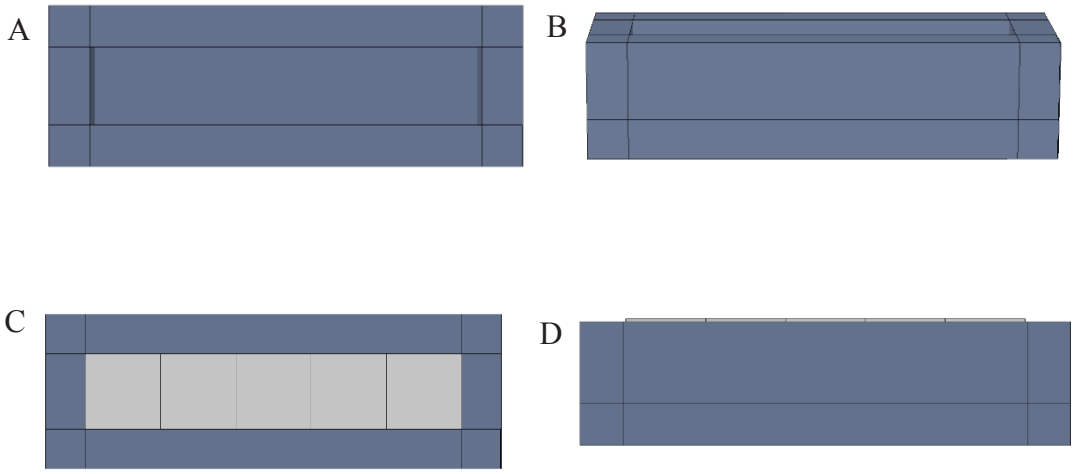

Figure 7. Illustration of the holder component. A, B) The top and side of view of only the component. C, D) The top and side view with magnets within the component.

2.4.3. Fabrication of Partial Gravity Cell Culture Platform with Halbach Array

All construction steps were combined to fabricate the partial gravity cell culture platform. First, the Halbach array is placed within the holder component, and the cell culture chamber is placed on the Halbach array to remain steady was bonded with tape. The partial gravity platform is ready to use in cell culture studies (Figure 8).

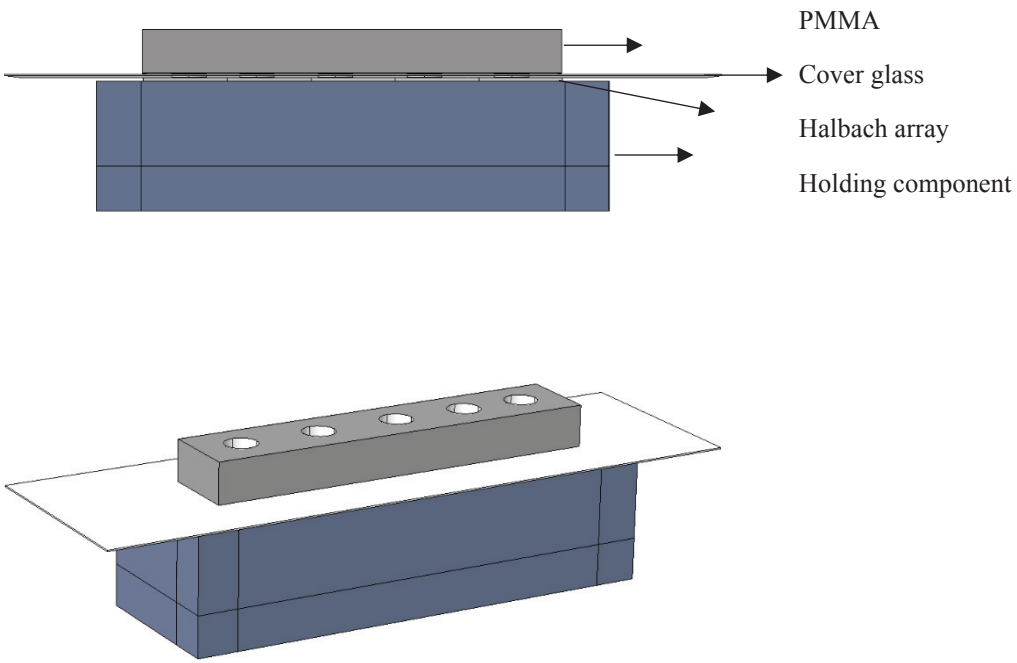

Figure 8. Illustration of front and side view of the design partial gravity platform.

2.5. Sedimentation of the Cells on Halbach Array Platform

To confirm whether the cells are sedimentation on the Halbach array system, sedimentation analysis was performed using determined Gd^{3+} concentrations (28 mM Gd^{3+} for Mars and 38 mM Gd^{3+} for the Moon). The Halbach array was placed inside the disc of the microscope. To observe cells, it was put a mirror at 45° on a stick properly as (Figure 9). Following, 7F2 cells were resuspended to 10^6 cells/ml using 0, 28, and 38 Mm Gd^{3+} concentration in the culture medium, approximately ~50 μL of cell suspension was loaded into a micro-capillary, and the capillary channel was placed above the Halbach array. To monitor sedimentation, images of cells were taken for 10 min every 1 min under the inverted microscope (Olympus IX-83), and the sedimentation velocity of the cells in the system was measured with TrackMate analysis of ImageJ Fiji.

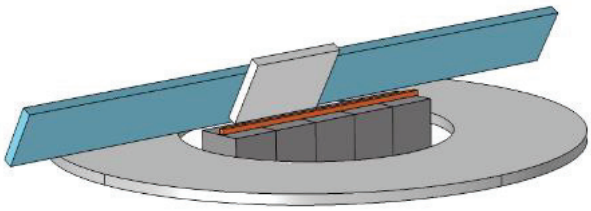

Figure 9. Illustration of the platform for sedimentation; the Halbach array is placed in the disk of an inverted microscope and a mirror is adjusted to 45° to monitor the cells in a capillary channel.

2.6. Cell Culture

7F2 (mouse osteoblasts, ATCC) were cultured in containing alpha minimum essential medium (αMEM) supplemented with 10% fetal bovine serum (FBS, Biological Industries) and 1% penicillin/streptomycin (Invitrogen) at 37°C in 5% CO_2 a humidified incubator. The growth medium was refreshed every 2-3 days. When cells reached approximately 80-90% confluence (every 4-6 days), the cells were passaged by using 0.25% trypsin-EDTA solution. The passage number of the cell culture was used to be between 6-15.

2.7. Cell Viability Assay

To examine the cytotoxicity effects of Gd^{3+} on cell viability, the cells were seeded at concentration $25x10^2$ cells/well in 96 well-plate and cultured for 7 days. After two days, for osteogenic induction, the growth medium (αMEM) was replaced with the osteogenic medium supplemented with 10 nM dexamethasone (Sigma), 50μg /mL ascorbic acid and 10 Mm β-glycerophosphate. Both growth and osteogenic cells were exposed to Gd^{3+} solution at 0, 28 mM, and 38 mM. The medium was refreshed 2-3 days by adding fresh Gd^{3+} solution, and cell viability was measured at 0, 3, and 7 days with

MTT assay (thiazolyl blue tetrazolium bromide). 0.5 mg/ml of MTT reagent (Amresco) was added to each well, and the plates were incubated at 37°C for 3 hours in the dark. The media was removed, 100 µl of DMSO was added to dissolve formazan crystals to each well, and coulometric measurements were performed at 570 nm and 690 nm.

2.8. Live/Dead Assay

The cells were seeded at $25x10^2$ cell/well into a 96-well plate and cultured for 7 days. After 2 days, the growth medium (aMEM) was replaced with the osteogenic induction medium containing 10 nM dexamethasone, 50µg /ml ascorbic acid, 10mM β-glycerophosphate for osteogenic differentiation. The growth and osteogenic cells were exposed to Gd^{3+} solution at 0, 28, and 38 mM. The medium was refreshed every 2-3 days by adding fresh Gd solution. Cell viability was assessed by live/dead assay (Calcein-AM/propidium iodide, Sigma Aldrich). On day 7, the cells were stained (for 1 ml PBS 2 µl Calcein-AM + 1 µl PI) for 15 min and imaged at 10x under the fluorescence microscope (Olympus IX-83).

To determine the impacts of simulated partial gravity on cell viability, the exposure of cells was to simulated partial gravity for 24 hours, and the cells were washed with PBS (one time) and incubated for 15 min with Calcein-AM/Propidium iodide dye and imaged under the fluorescence microscope (Olympus IX-83).

2.9. Osteogenic Differentiation

The cells were seeded at concentration $1x10^3$ cell/well into 6-well plate. After 2 days, the standard medium was replaced with the osteogenic induction medium containing 10 nM dexamethasone, 50 mg/mL ascorbic acid, and 10 mM β-glycerophosphate, and the cells were cultured for 14 days [90]. Calcium deposits, a final indicator of the differentiated osteoblasts, were assessed by Alizarin Red S (Sigma Aldrich) staining at the 14^{th} of the culture [91].

2.10. Actin Cytoskeleton Staining

To investigate changes in F-actin filaments and nucleus under simulated partial gravity, the cells were stained with phalloidin/dapi. Phalloidin (green) (Alexa 488) stains F-actin filaments of the cells, while dapi (blue) stains nucleus of the cells. On the 16^{th} of osteogenic differentiation, the cells were trypsinized and seeded at 15 x 10^3 cells/well in15 µl for the Moon and in 25 µl for Mars to the cell culture chamber and exposed to simulated partial gravity for 24 hours. Following 24 h, the cells fixed the surface with paraformaldehyde and were stained with phalloidin-dapi dye for 45-60 min and imaged 20x under the fluorescence microscope (Olympus IX-83).

2.11. Simulated Partial Gravity with Halbach Array

To mimic the Lunar and Martian gravity, the number of the cells was determined as at concentration 15 x 10^3 cells/well in15 µl and 25 µl, respectively. Initially, the osteogenic differentiated 7F2 cells were trypsinized and were collected using a scraper to a falcon tube at the 14^{th} day of culture, and 15 x 10^3 cells were seeded into each well, including 28 mM Gd^{3+} for Mars and 38 mM Gd^{3+} for the Moon. The cell culture chamber was placed over the Halbach array. Also, the cells were seeded at the same concentration without $Gd^{3+}$for positive and negative control. However, for positive control, the cells were placed over the Halbach array without Gd^{3+} to distinguish between the effects of partial gravity and the magnetic field. The cells were incubated for 24 hours at 37°C and 5% CO_2 incubator with dH_2O to reduce evaporation in the culture dish (Figure 10).

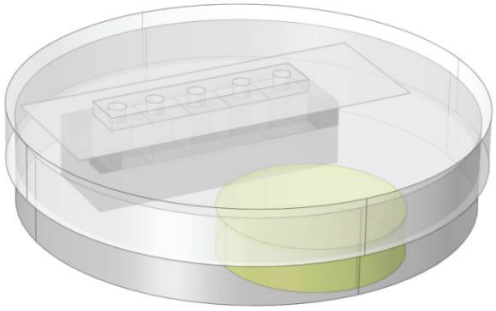

Figure 10. Illustration of the cell culture setup. The culture chamber with Halbach array is placed in a 10 cm culture plate, including dH_2O in a 3 cm culture dish to reduce evaporation.

2.12. Statistical Analysis

All experiments were repeated at least three times. Data are expressed as the mean ± standard deviation. Statistical analysis was performed by an unpaired Student's t-test and one-way analysis of variance. Also, multiple regression statistical analysis was conducted prediction the value of a variable based on the value of two or more other variables. Statistical difference was considered as $P < 0.05$. $P < 0.01$, $P < 0.001$ and $P < 0.0001$ were noted as "**, "***" and ''****'', respectively.

To determine culture platform position, multiple regression methods based on simulation results were used. Multiple regression is a statistical analysis technique based on the relationship between one dependent variable and several independent variables. The multiple regression equations the following:

$$y = \beta 0 + \beta 1x1 + \beta 2x2 + \ldots + \beta nxn. \quad (4)$$

y is dependent variable, β0 is an intercept, x1, x2., are independent variables, and β1, β2., are slopes. Many simulation data were obtained according to the gravitational acceleration equation, and there were known variables such as the density of cells in this study, hence for this purpose, multiple regression analysis was performed to estimate the

required Gd^{3+} concentrations to mimic the partial gravity of the lunar and Martian. The dependent variable was used as the peak value of the gravitational acceleration at different heights of the cell culture chamber from the magnets and at different cell densities by performed simulations data, while the independent variables were as known densities of cells and the height of the cell culture chamber from the magnets that heights were identified according to the glass thickness.

CHAPTER 3

RESULTS AND DISCUSSION

3.1. Simulations of the Designed Halbach Array

In this study, it was used five N52 cubes of neodymium magnets (9.525 mm) and designed the Halbach array (Figure 11). Brmax value of the magnets is 14.800 Gauss was converted to kiloampere per meter (kA/m), and the magnetization value was founded as 1177 kA/m. Subsequently, a suitable mesh was performed to accurate the finite element method. The mesh is the most important step in the finite element method to simulate the design because the lower the mesh value, the more accuracy of simulation increases. The mesh size of magnets was 20 μm of maximum and 1 μm of minimum, while air space was 88 μm of maximum and 3 μm of minimum was identified. The mesh pattern was triangular (Figure. 12). Finally, the Halbach array simulations were carried out based on finite element method (FEM).

Figure 11. 2D view of the Halbach array design consisting of five neodymium magnets.

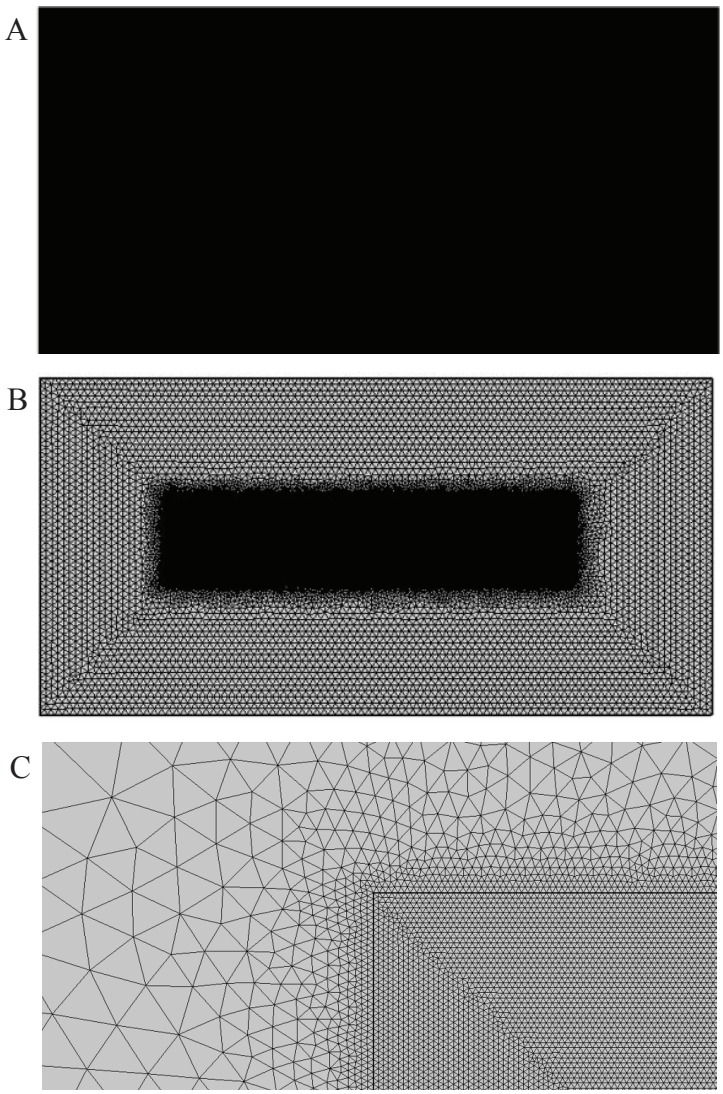

Figure 12. A) The triangular pattern of the mesh of five magnets and mesh sizes of magnets are 20 μm of max and 1 μm of minimum and air space of mesh size are 88 μm and 3 μm, respectively based on finite element methodology. B, C) Zoomed view of the mesh pattern of the magnets and the air space.

3.2. Simulations of Magnetic Flux Density of the Designed Halbach Array

The magnetic flux density is measured in Tesla (T). Based on finite element model (FEM) simulations, the high or low magnetic field side of the Halbach array has been determined. According to the simulation results, the top surface of the Halbach array was identified as the test surface to mimic partial gravity due to the high magnetic field. The magnetic field in points of the junction of magnets was about 2 Tesla, while the top surface of the magnets was about 1 Tesla (Figure 13).

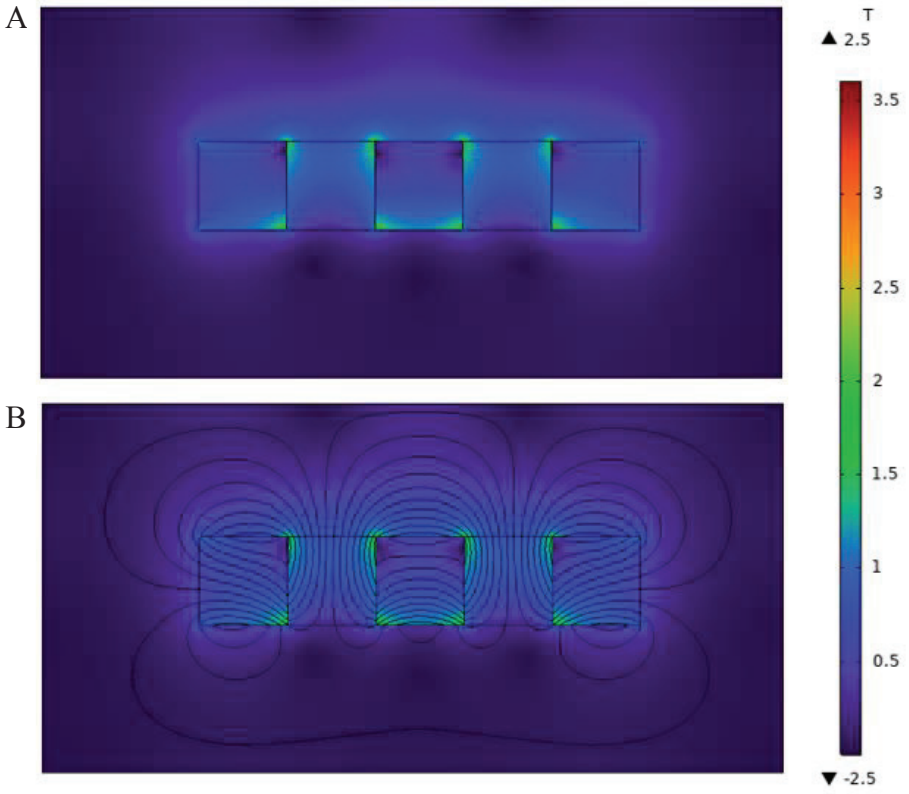

Figure 13. A) Magnetic flux density norm (Tesla) image of the Halbach array. B) Image of streamlines of magnetic flux density around the Halbach array via finite element method.

3.3. Simulations of Magnetic force (F_{mag}) and Gravitational force (F_g)

According to the determined simulation test surface, the simulations were performed based on equation 1 using finite element method. Here, it was aimed to identify whether the cells were levitation. For this purpose, it was preferred 5 mM, 10 mM, 20 mM, 40 mM, and 80 mM Gd^{3+} concentrations, 1.02 g mL^{-1}, 1.06 g mL^{-1}, and 1.1 g mL^{-1} densities of cells, and 150 µm, 300 µm, 450 µm, and 600 µm of heights. According to the simulation results, when 80 mM Gd^{3+} was used, cells are levitated at all cell densities. However, when using less than 40 mM Gd^{3+}, the cells were not levitated. In 1.02 g mL^{-1} cells sedimented only when using 5 mM and 10 mM Gd^{3+}. The cells with 1.06 g mL^{-1} density did not levitate at 5, 10 and 20 mM Gd^{3+}, whereas in 1.1 g mL^{-1} cells did not levitate at 5, 10, 20, and 40 mM Gd^{3+}. If F_{mag} value is higher than F_g value, the cells are levitated, this condition is not useful for our study because F_g value should be higher than F_{mag} to sediment of the cells at different Gd^{3+} concentrations. Therefore, it can be used Gd^{3+} concentrations that are between 5 mM Gd^{3+} and 20 mM Gd^{3+} in the cells with ~1.06 g mL^{-1} density (Figures 14-17).

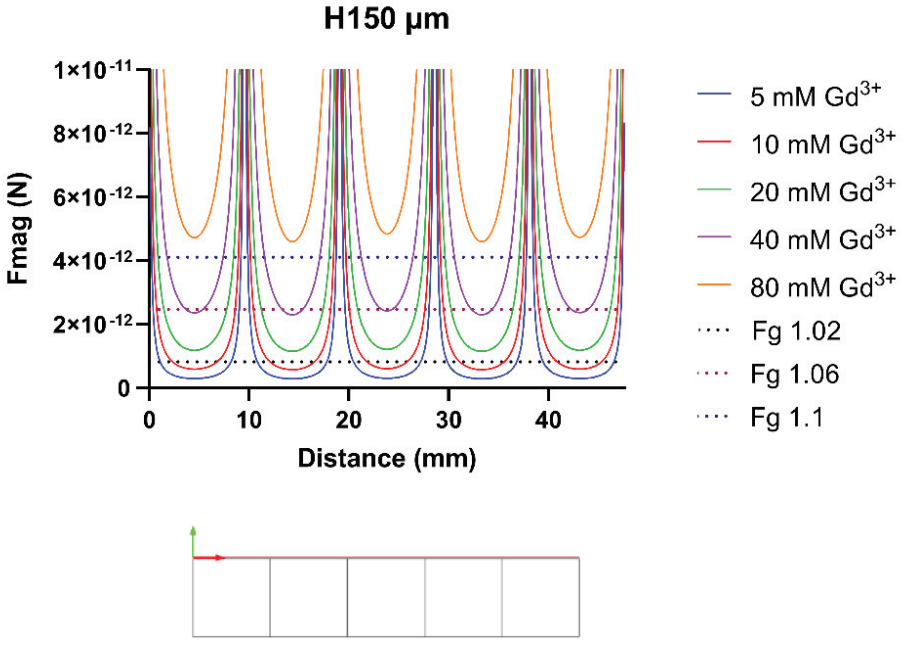

Figure 14. The configuration of the relationship between magnetic force and gravitational force (at different densities of cells 1.02 g mL^{-1}, 1.06 g mL^{-1}, and 1.1 g mL^{-1} and different Gd^{3+} concentrations at 5, 10, 20, 40, and 80 mM) at the height of 150 µm from the Halbach array.

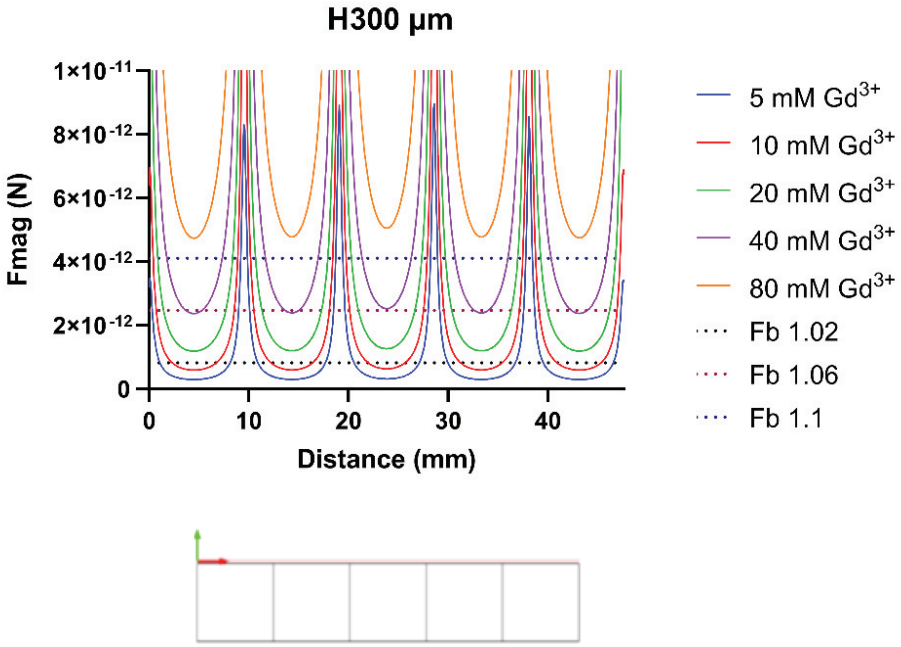

Figure 15. The configuration of the relationship between magnetic force and gravitational force (at different densities of cells 1.02 g mL^{-1}, 1.06 g mL^{-1}, and 1.1 g mL^{-1} and different Gd^{3+} concentrations at 5, 10, 20, 40, and 80 mM) at the height of 300 µm from the Halbach array.

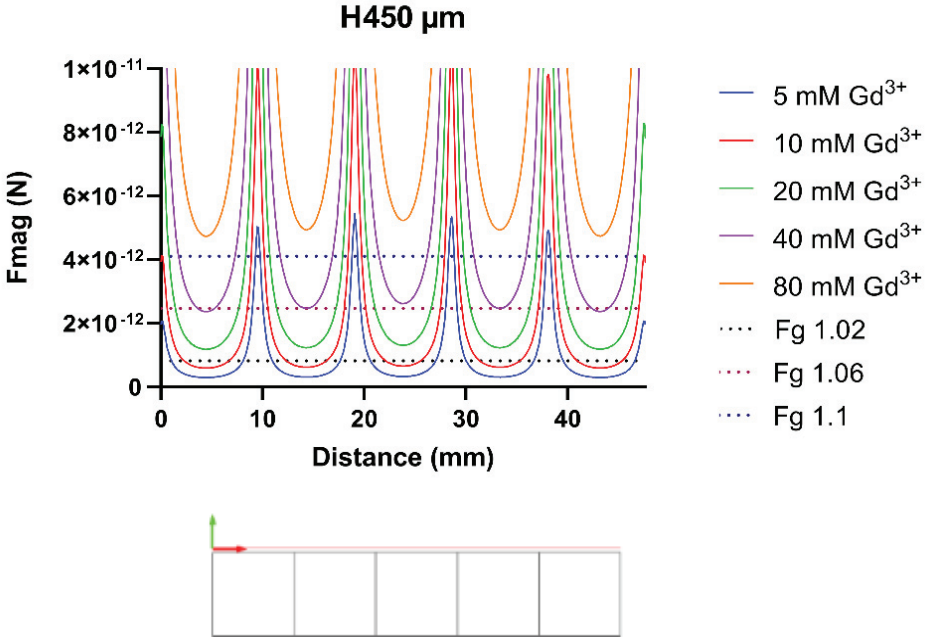

Figure 16. The configuration of the relationship between magnetic force and gravitational force (at different densities of cells 1.02 g mL^{-1}, 1.06 g mL^{-1}, and 1.1 g mL^{-1}

and different Gd^{3+} concentrations at 5, 10, 20, 40, and 80 mM) at the height of 450 µm from the Halbach array.

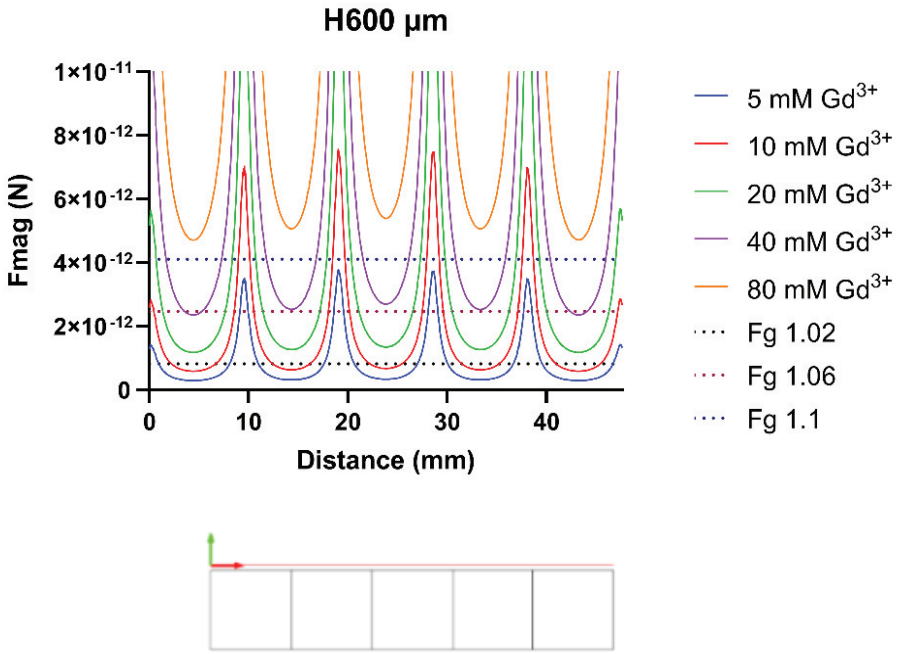

Figure 17. The configuration of the relationship between magnetic force and gravitational force (at different densities of cells 1.02 g mL^{-1}, 1.06 g mL^{-1}, and 1.1 g mL^{-1} and different Gd^{3+} concentrations at 5, 10, 20, 40, and 80 mM) at the height of 600 µm height from the Halbach array.

3.4. Simulations of Gravitational Acceleration

Gravitational force of Earth can be manipulated by benefit its magnitude or direction. Therefore, in this study, it was manipulated benefited its magnitude to reduce gravitational acceleration by using a magnetic field. Earth's gravitational acceleration was declined based on the acceleration formula shown in equation 3. For this, it was used different Gd^{3+} concentrations that are 5 mM, 10 mM, and 20 mM, and known cell densities, in addition to also by selecting different height levels above the Halbach array of the cell culture chamber of 150 µm, 300 µm, 450 µm and 600 µm heights. According to the simulations, when 5 mM Gd^{3+} was used, the gravitational acceleration reduced

about 8 m/s^2 in 1.06 and 1.1 g mL^{-1} density whereas it decreased about 6 m/s^2 in 1.02 mL^{-1} density at 150 µm height from Halbach array (Figure 18). In addition to this, as increases Gd^{3+} concentration, the acceleration reduced nearly 5-6 m/s^2 in 1.06 g mL^{-1} and 1.1 g mL^{-1} density, while about 2-3 m/s^2 in 1.02 g mL^{-1} density (Figures 18-29).

However, the expected gravitational acceleration of the lunar and Martian could not be specifically determined. Therefore, the required Gd^{3+} concentrations for the Moon and Mars accelerations values were predicted with multiple regression analysis.

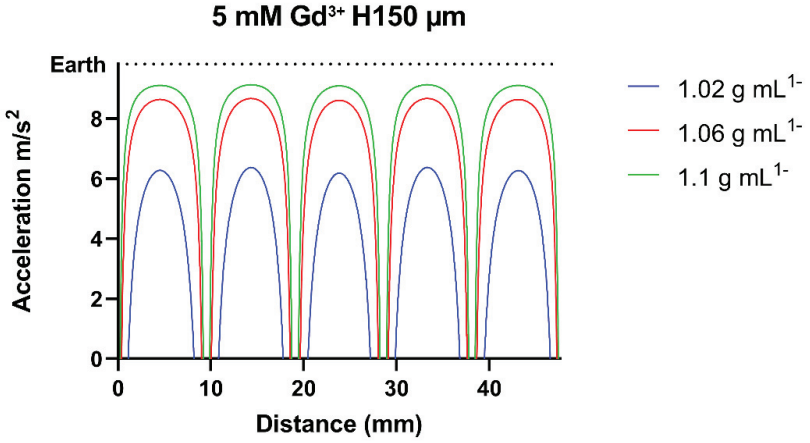

Figure 18. Configuration of the reduced gravitational acceleration of Earth in different densities of cells (1.02, 1.06, and 1.1 g mL $^{-1}$) when using 5 mM Gd^{3+} solution at 150 µm height from Halbach array.

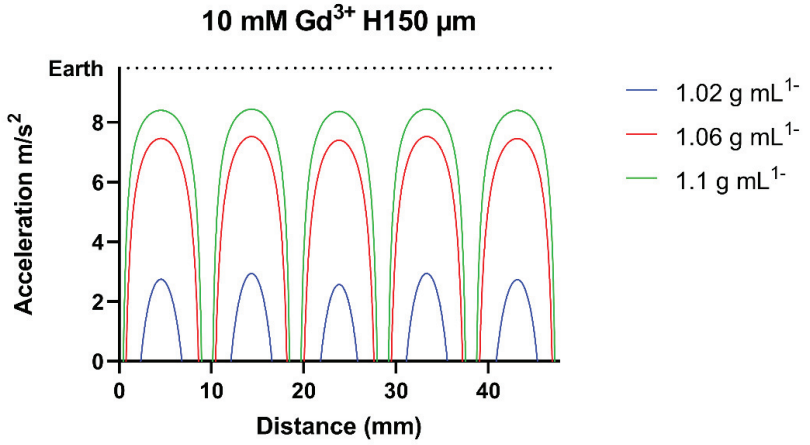

Figure 19. Configuration of the reduced gravitational acceleration of Earth in different densities of cells (1.02, 1.06, and 1.1 g mL $^{-1}$) when using 10 mM Gd^{3+} solution at 150 µm height from Halbach array.

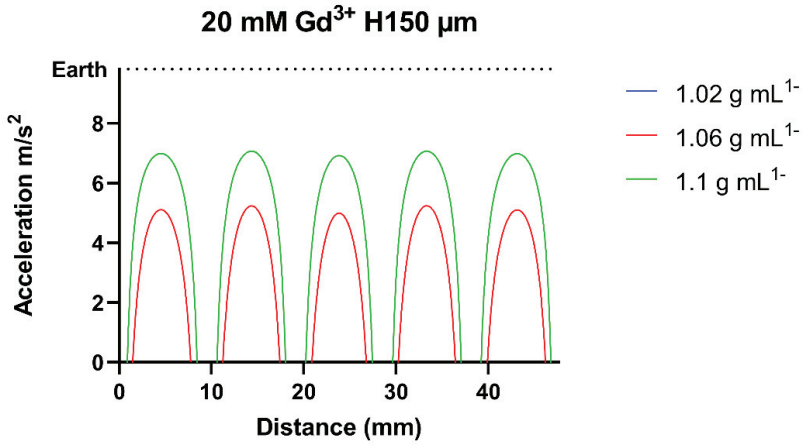

Figure 20. Configuration of the reduced gravitational acceleration of Earth in different densities of cells (1.02, 1.06, and 1.1 g mL $^{-1}$) when using 20 mM Gd^{3+} solution at 150 µm height from Halbach array.

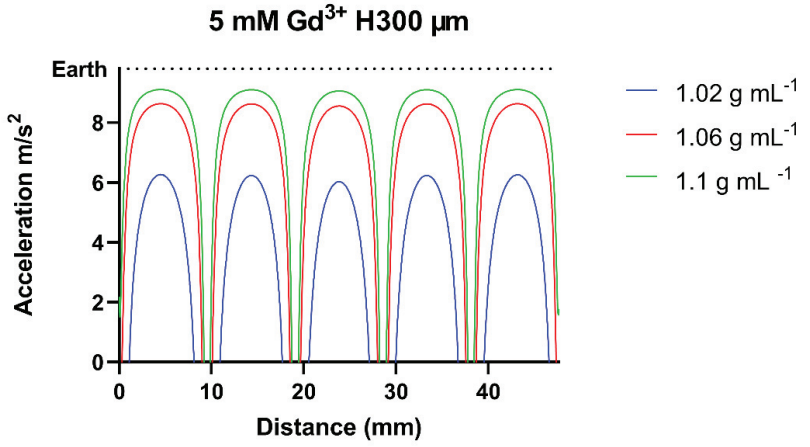

Figure 21. Configuration of the reduced gravitational acceleration of Earth in different densities of cells (1.02, 1.06, and 1.1 g mL $^{-1}$) when using 5 mM Gd^{3+} solution at 300 µm height from Halbach array.

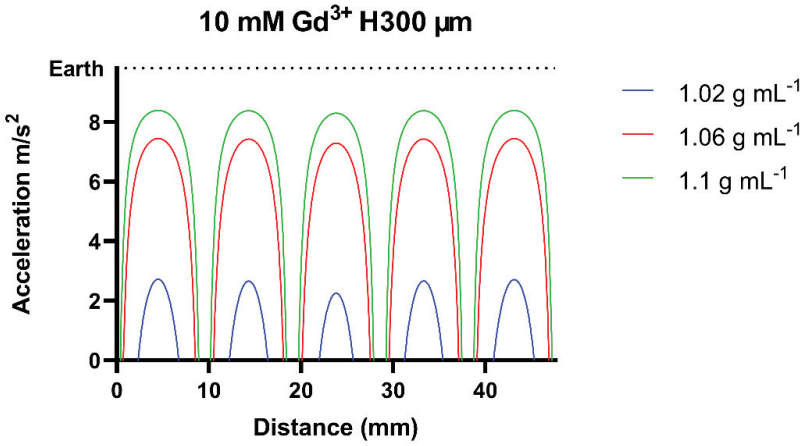

Figure 22. Configuration of the reduced gravitational acceleration of Earth in different densities of cells (1.02, 1.06, and 1.1 g mL $^{-1}$) when using 10 mM Gd^{3+} solution at 300 µm height from Halbach array.

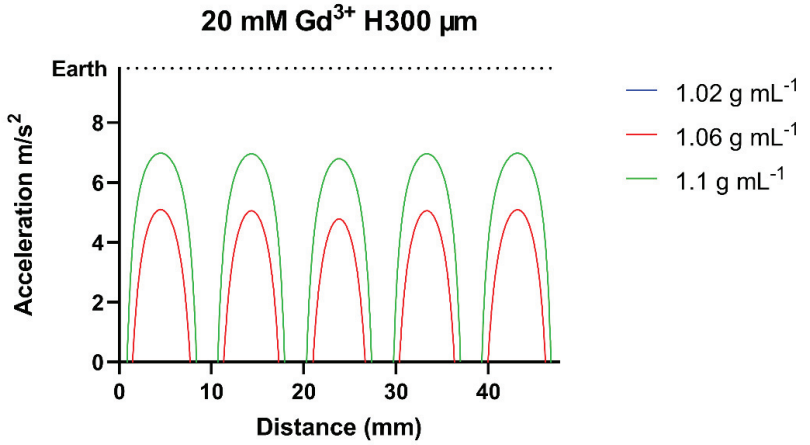

Figure 23. Configuration of the reduced gravitational acceleration of Earth in different densities of cells (1.02, 1.06, and 1.1 g mL $^{-1}$) when using 20 mM Gd^{3+} solution at 300 µm height from Halbach array.

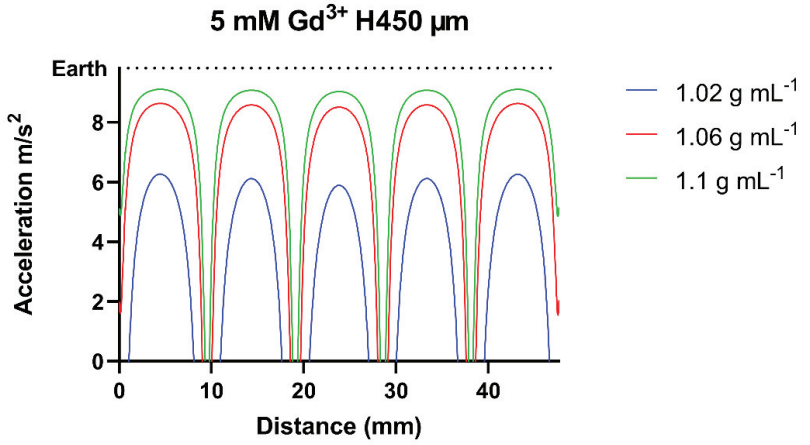

Figure 24. Configuration of the reduced gravitational acceleration of Earth in different densities of cells (1.02, 1.06, and 1.1 g mL $^{-1}$) when using 5 mM Gd^{3+} solution at 450 µm height from Halbach array.

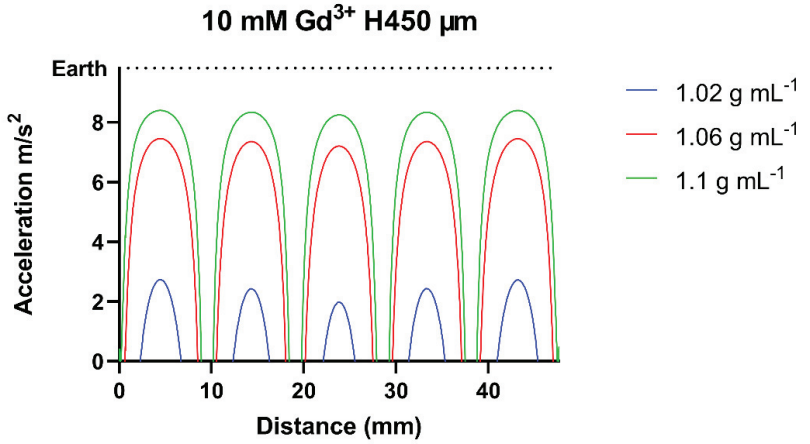

Figure 25. Configuration of the reduced gravitational acceleration of Earth in different densities of cells (1.02, 1.06, and 1.1 g mL $^{-1}$) when using 10 mM Gd^{3+} solution at 450 µm height from Halbach array.

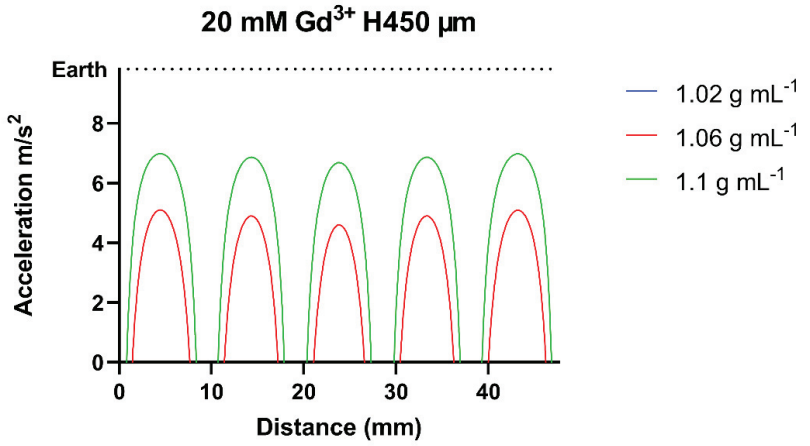

Figure 26. Configuration of the reduced gravitational acceleration of Earth in different densities of cells (1.02, 1.06, and 1.1 g mL $^{-1}$) when using 20 mM Gd^{3+} solution at 450 µm height from Halbach array.

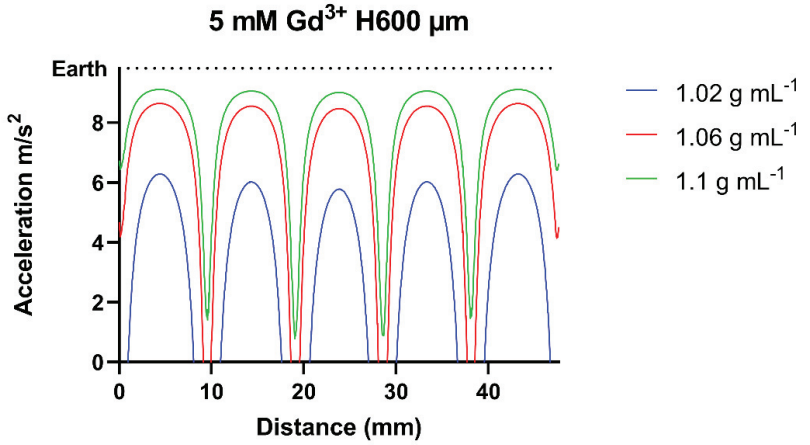

Figure 27. Configuration of the reduced gravitational acceleration of Earth in different densities of cells (1.02, 1.06, and 1.1 g mL $^{-1}$) when using 5 mM Gd^{3+} solution at 600 µm height from Halbach array.

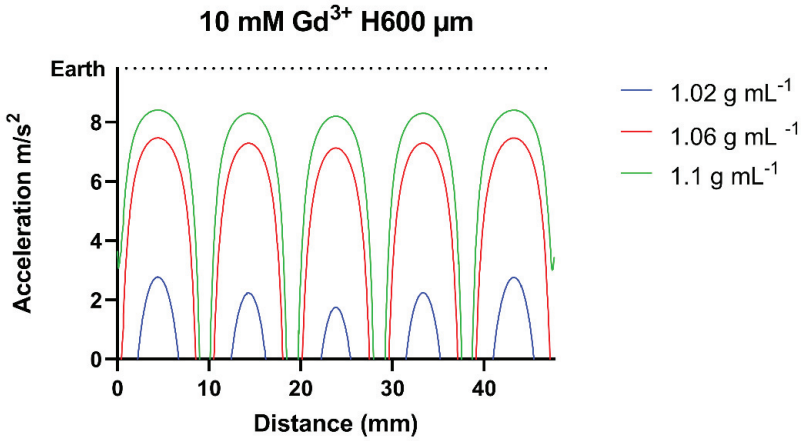

Figure 28. Configuration of the reduced gravitational acceleration of Earth in different densities of cells (1.02, 1.06, and 1.1 g mL $^{-1}$) when using 10 mM Gd^{3+} solution at 600 µm height from Halbach array.

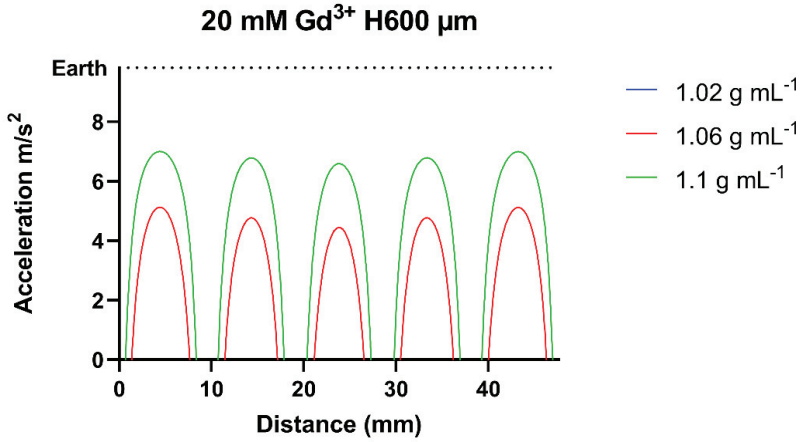

Figure 29. Configuration of the reduced gravitational acceleration of Earth in different densities of cells (1.02, 1.06, and 1.1 g mL $^{-1}$) when using 20 mM Gd^{3+} solution at 600 µm height from Halbach array.

3.5. Prediction of Required Gd^{3+} Concentrations to Mimic Partial Gravity of the Moon and Mars

The multiple regression analysis is used to predict the relationship between a single dependent variable and several independent variables; therefore, known data that cell density, gravitational acceleration values of the Moon (1.6 m/s^2) and Mars (3.7 m/s^2), and heights of culture chamber from the platform due to the thickness of the cover glass were considered. As specific Gd^{3+} concentrations could not be determined to simulate the partial gravity, a multiple regression analysis was performed to predict required Gd^{3+} concentrations to simulate reduced gravity. According to our multiple regression model, the dependent variable values were chosen as peak points of the acceleration at different heights and densities of cells. The independent variables used height values categorically at 0, 150, 300, 450, and 600 μm. The other independent values that is continuous were used at densities of cells of 1020, 1060, and 1100 kg/m^3 and 5 mM, 10 mM, and 20 mM Gd^{3+} concentrations. As a result, a total of 184 data was obtained, and there was a significant relationship between gravitational acceleration, cell density, and Gd^{3+} concentration ($p^{****} < 0{,}0001$), whereas no significant difference was observed between acceleration and height. R^2 was 0.8003 and this showed high relationship between acceleration and Gd^{3+} concentrations or density. There was positive correlation between Gd^{3+} concentrations and density, while between the acceleration and Gd^{3+} concentration was negative correlation. The multiple regression equation is as follows:

$$\text{Acceleration}\left(\frac{\text{m}}{\text{s2}}\right) \sim \text{Intercept} + \text{Density}\left(\frac{\text{kg}}{\text{m3}}\right) + \text{Gd concentration (mM)} + \text{Height (μm)} \quad (4)$$

Parameter estimates	Variable	Estimate	P value	P value summary
β0	Intercept	-49.51	<0,0001	****
β1	Density kg/m3	0.05496	<0,0001	****
β2	Gd concentration mM	-0.2007	<0,0001	****
β3	Height μm[150]	-0.02136	0.9287	ns
β4	Height μm[300]	-0.0919	0.7002	ns
β5	Height μm[450]	-0.1508	0.5278	ns
β6	Height μm[600]	-0.2	0.4024	ns

Figure 30. Table of the result of multiple regression analysis.

For 7F2 cells, known independent variables were the densities of cells (1070 kg/m^3) and preferred 150 μm height, and the dependent variables were the acceleration of the Moon (1.6 m/s^2) and Mars (3.7 m/s^2); According the analysis results, required Gd^{3+} concentrations for the Moon and Mars were determined to be 38 mM and 28 mM Gd^{3+}, respectively. The calculation of the required Gd^{3+} concentration to mimic partial gravity of the lunar according to multiple regression analysis results (Figure 30). Also, in figure 31 shows that the acceleration was reduced at about 1.6 m/s^2 when used predicted 38 mM Gd^{3+}.

Moon	Value
Acceleration m/s^2	1.6
İntercept	-49.51
β1*Density (1070 kg/m^3)	58.8072
β3*Height μm [150]	-0.02136
Sum	9.27584
Acceleration-Sum	-7.67584
Required Gd^{3+} concentrations	38.24

Figure 31. An example of multiple regression analysis for 7F2 cells. To simulate reduced gravity for the Moon is needed 38 mM Gd^{3+} concentration.

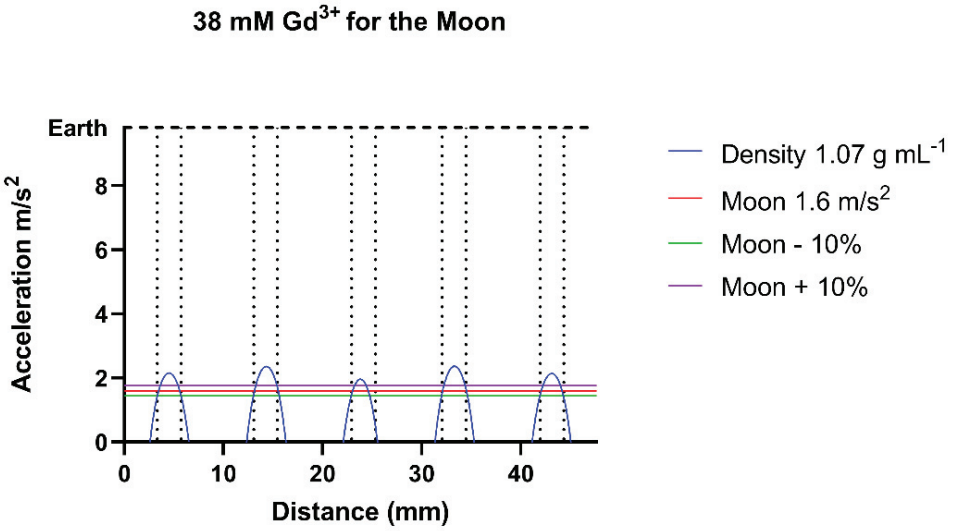

Figure 32. The graph shows that when the density of the cells is 1.07 g mL^{-1} and the Gd^{3+} concentration is 38 mM, the gravity of the Earth (9.81 m/s^2) is approximately reduced to that of the Moon's gravity (1.6 m/s^2).

3.6. Cell Culture Chamber Design Based on Determined Simulations

To simulate the fractional gravity of Mars and the Moon, the gravitational range was determined as ±10% of the 3.7 m/s^2 for Mars and 1.6 m/s^2 for the Moon. For this purpose, the diameters of the culture wells were determined as 3 mm for Mars and 2.4 mm for the Moon. Each cell culture well was positioned between beginning and end points of green horizontal line. For Mars, these points were between 3- 6 mm for the first well, 12.8-15.8 mm for the second well, 22.6-25.6 mm for the third well, 31.8-34.8 mm for the fourth well, and 41.6-44.6 mm fifth well. For the Moon, 1st well was between 3.33-5.73 mm, 13.05-15.45 mm, 22.93-25.33 mm, 32.06-34.46 mm, and 41.94- 44.34 mm 2nd, 3rd, 4th, and 5th respectively. The figure below shows the places of culture wells between two vertical dotted lines according to the green horizontal line (Figures 33-34).

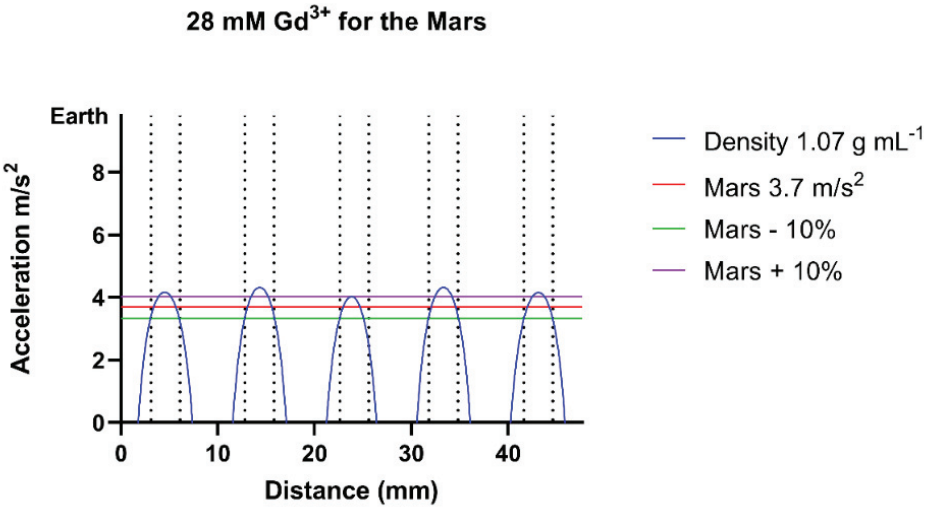

Figure 33. The Martian culture chamber's place was determined by the distance of the green line between dotted lines.

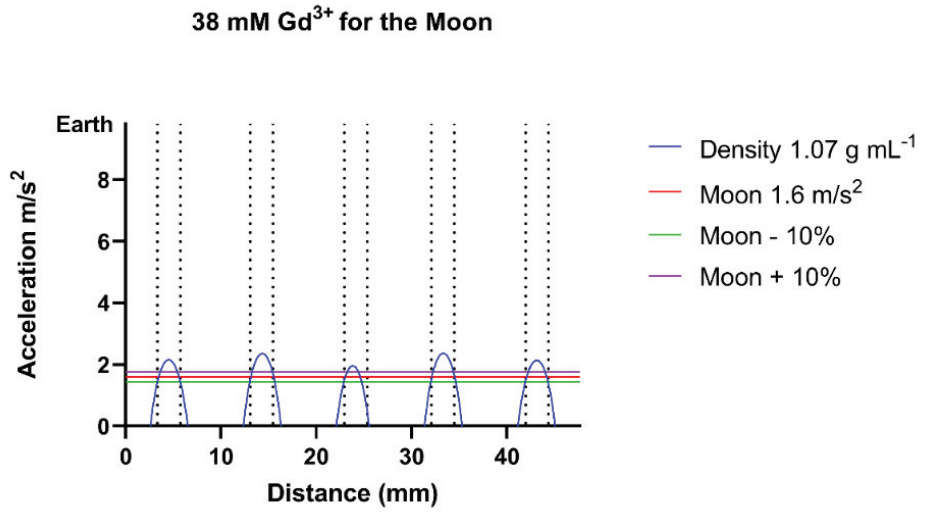

Figure 34. The Lunar culture chamber's place was determined by the distance of the green line between dotted lines.

3.7. Sedimentation Analysis with TrackMate of ImageJ Fiji

After the simulations and model selection, we first aimed to analyze whether the sedimentation rate (velocity) of 7F2 cells and the gravitational acceleration on the cells decreased at the determined Gd^{3+} concentrations on the Halbach array. To confirm the sedimentation of the cells at 0, 28 and 38 mM Gd^{3+} was taken images sedimentation of the cells under an inverted microscope for 10 minutes. Taken images have been concatenated as a video in the ImageJ program. Then, the velocity of sedimentation of the cells was analyzed with TrackMate. According to the velocity results, the cells in the control group were sedimentation within 4 minutes (Figure. 37), and the mean velocity value was 8.07 m/s^2. Moreover, the cells exposed to 28 mM Gd^{3+} experiment group had slower sedimentation than the control group, and the sedimentation velocity was 6.87 m/s^2 and there was a significant difference with respect to the control group ($p = 0.00007$ ***). On the other hand, the cells exposed to 38 mM Gd^{3+}, were become the slowest sedimentation among the groups and the velocity of the sedimentation was 6.63 m/s^2, and it was observed statically significant difference compared with the control ($p = 0.0001$****). The results confirmed the sedimentation of the cells on the Halbach array platform at determined Gd^{3+} concentrations. Moreover, 3D images of the cells show that the cells in the control group were sedimentation within 4 minutes, whereas the cells exposed to 28 and 38 mM Gd^{3+} cells still had not all sedimented because more time was needed for the sedimentation of all cells. These results were shown that the acceleration of cells was reduced.

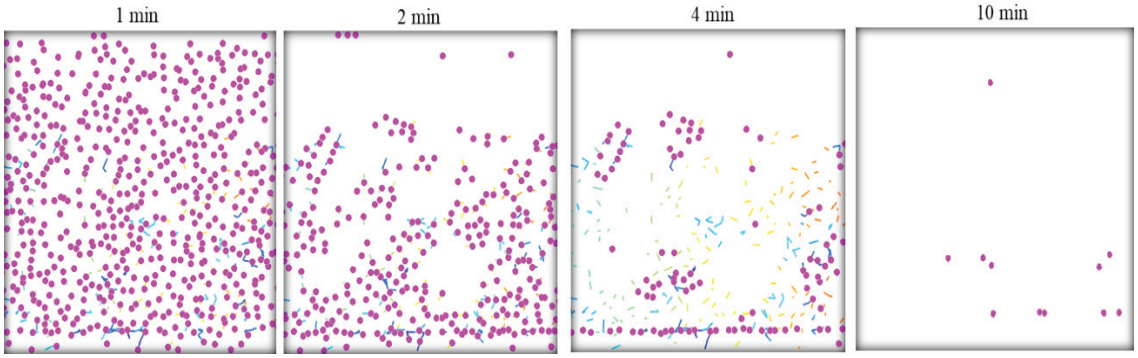

Figure 35. 2D view of sedimentation analysis of 7F2 cells at 0 Mm Gd^{3+} concentration after 1, 2, 3 and 4 min and all cells were sedimented at 10 minutes.

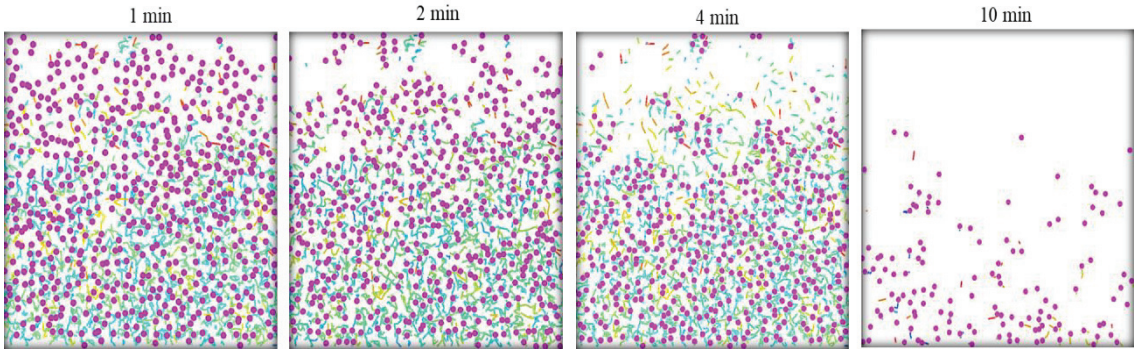

Figure 36. 2D view of sedimentation analysis of 7F2 cells at 28 Mm Gd^{3+} concentration after 1, 2,4, and 10 minutes. However, all cells were not sedimented within 10 minutes.

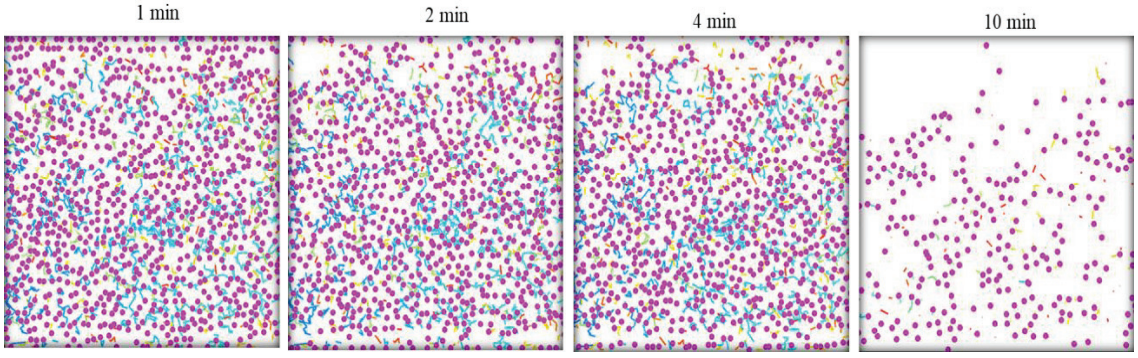

Figure 37. 2D view of sedimentation analysis of 7F2 cells at 38 Mm Gd^{3+} concentration after 1, 2,4, and 10 minutes. However, all cells were not still sedimented within 10 minutes.

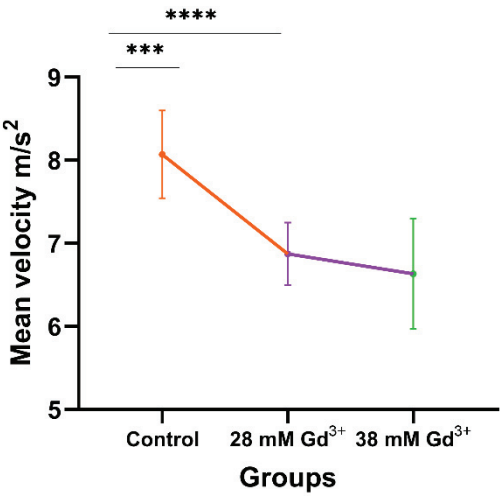

Figure 38. Sedimentation mean velocity of 7F2 cells analysis results show 8.07 m/s^2, 6.87 m/s^2, and 6.63 m/s^2 at 0 mM, 28 mM, and 38 mM Gd^{3+} concentrations, respectively. There was a statistically significant difference between 28 mM Gd^{3+} and the control group (n=3, p = 0.0007 ***) and 38 mM Gd^{3+} and the control group (n=3, p < 0.0001 ****) with unpaired Student T-test and one-way ANOVA.

3.8. Determination of cytotoxicity effects of 28 mM and 38 mM Gd^{3+} on cell viability of the 7F2 cells

Initially, the cytotoxic effect of the determined Gd^{3+} (0, 28 and 38 mM) concentrations on cell viability of the 7F2 cells induced with growth and osteogenic medium were assessed with an MTT assay at 0, 3, and 7 days of culture. Also, Cell viability was visualized by live-dead staining (Calcein/PI) only 7^{th} days of culture. These experiments were performed in a 96-well plate. The cell proliferation was normalized to zero days of the culture. In growth groups, cell proliferation in control groups increased 9-fold and 19-fold at 3 and 7 days, respectively, in growth cells exposed to 28 mM Gd^{3+}, the proliferation increased 8-fold at 3 days and 16-fold at 7 days, whereas exposed to 38 mM Gd^{3+} the cells increased 8-fold at 3 days and 18-fold at 7 days. There was no significant difference between untreated and treated Gd^{3+} growth groups (Figure 39). On the other hand, osteogenic cells showed a similar fold change in cell proliferation versus control groups. In the osteo control cells, the cell proliferation increased 6-fold at 3 days

and 16-fold at 7 days of culture. The exposed to 28 and 38 Mm Gd^{3+} osteo cells showed a 6-fold and 15-fold increase at 3 days and 7 days of the culture (Figure 40). In briefly, the bar graphs show a decreased proliferation in treated Gd^{3+} groups versus control groups, however, there was no observed statistically significant difference between the experimental and control groups. In addition, the cell viability was assessed with live-dead staining (Calcein/PI). However, as the analysis of live cells was difficult, number of dead cells were analyses at 0.94 mm^2 with ImageJ Fiji. According to the results, the confluence of live cells in control groups was similar compared to treated Gd^{3+} groups, and there was no statistically significant difference number of dead cells at 0.94 mm^2 in all groups at 7 days of culture (n=3 ns, Figure 42).

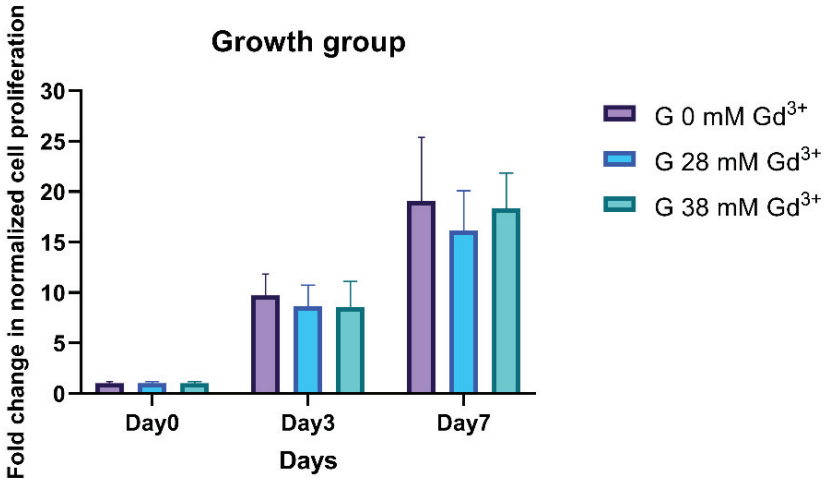

Figure 39. Cell viability of 7F2 cells was no affected exposed to 28 mM Gd^{+3} concentrations at days 0, 3 and 7 of culture. There was no significant difference between the viability of 28 mM and 38 mM Gd^{3+} groups and controls.

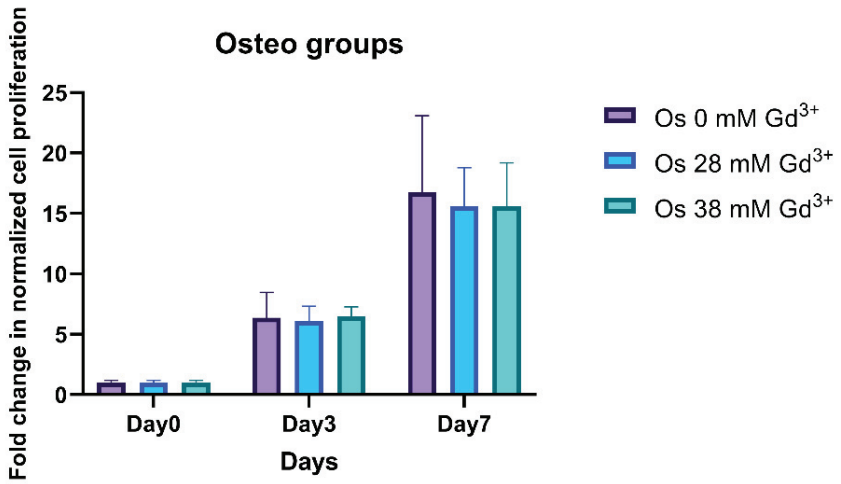

Figure 40. Cell viability of 7F2 cells was no affected exposed to 28 mM Gd^{+3} and 38 mM Gd^{+3} concentrations at days 0, 3 and 7 of culture. There was no significant difference between the viability of 28 mM and 38 mM Gd^{3+} groups and controls.

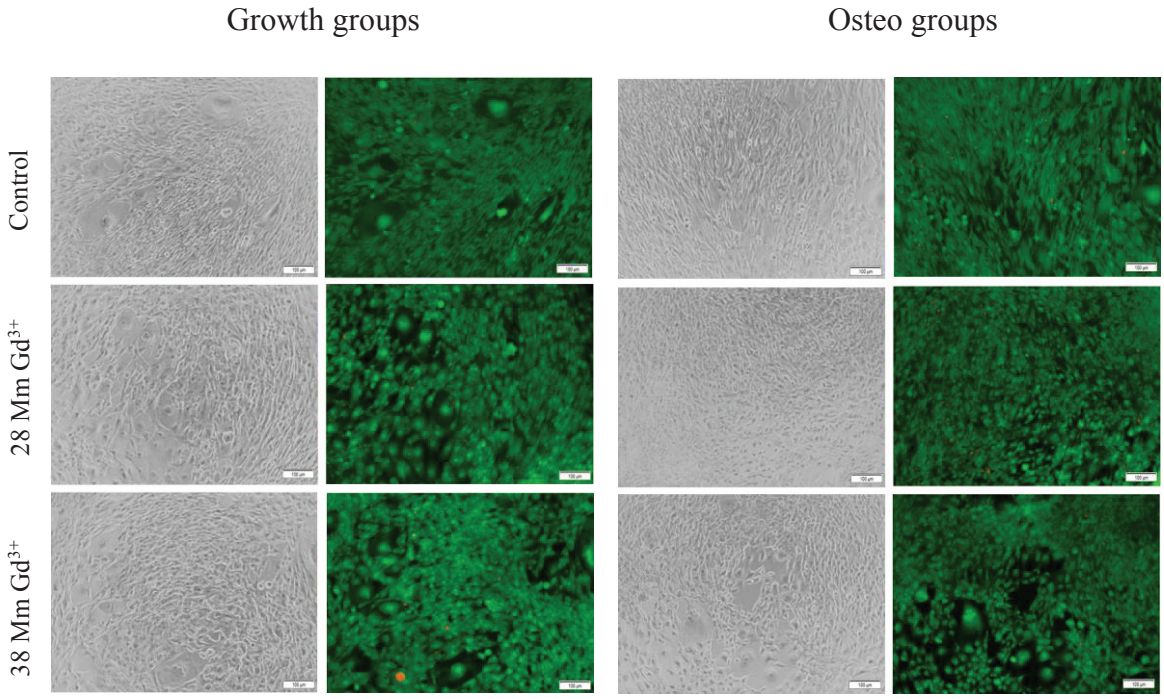

Figure 41. Images of live/dead staining of growth and osteogenic of 7F2 cells exposed to 0, 28 and 38 mM Gd^{3+} concentrations at 7^{th} days. Scale bar: 100 µm.

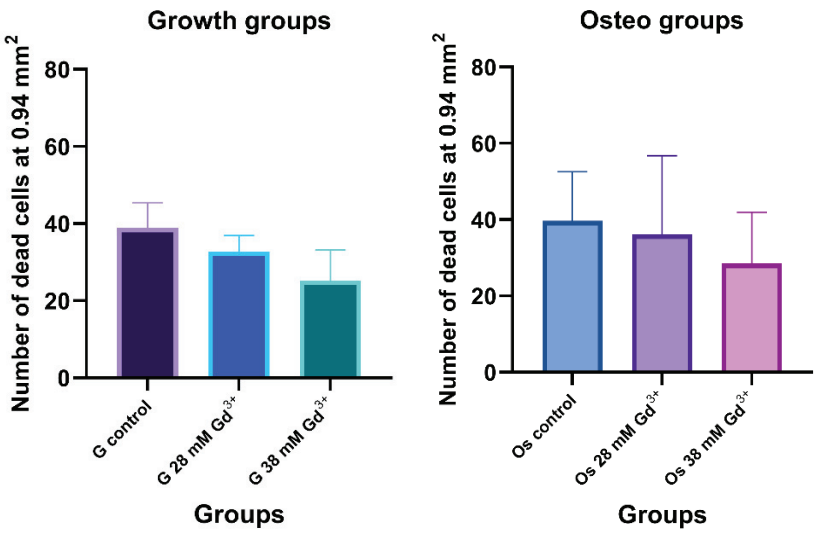

Figure 42. Number of dead cells at 0.94 mm^2 exposed to 0, 28, and 38 mM Gd^{3+} concentrations on the 7th day of culture. There was no observed significant difference between groups.

Gadavist (Gd^{3+}) is extensively used in magnetic levitation research due to being a paramagnetic agent and cytotoxicity effects on the cells are crucial. Different types of cells were exposed to several Gd^{3+} concentrations. D1-ORL-UVA exposed to 100 mM Gd^{3+} for 24 h exhibited similar viability compared to control groups [92]. Esophageal Adenocarcinoma (JHESoAD1) cells exposed to different concentrations of 0, 30, 50, and 100 mM Gd^{3+} showed similar cell viability with respect to control groups for 5 days [93]. Also, the viability of NIH 3T3 cells had not been influenced exposed to 100 Mm Gd^{3+} for 3 days, but it caused a reduction of cell proliferation when used ≥75 mM Gd^{3+} concentrations[94,95]. Our results showed similarity to other studies, and it was concluded that determined Gd^{3+} concentrations were not affected the cell viability of 7F2 cells during 7 days of culture.

3.9. Determination of Effects of Simulated Partial Gravity on Cell Viability of 7F2 cells

First, to examine the impact of partial gravity on the attachment of the cells on the culture chamber surface for 24 hours, it was cultured 7F2 cells in a culture chamber with 28 mM Gd^{3+} (Mars) and 38 mM Gd^{3+} (Moon) concentrations, and after 24 h, it was taken phase images. The results showed that positive and negative control had a similar confluency of the cells, while Mars and Moon had less confluency of the cells compared to control groups (Figure 43).

In order to determine the impact of simulated partial gravity on cell viability for 24 h, the cell viability was assessed by live/dead staining (Calcein-AM/PI). Green cells are live cells, while red cells are dead cells (Figure 43). The number of dead cells were calculated by ImageJ Fiji at 0.94 mm^2. Results showed the greatest number of dead cells was in Moon groups, but there was no significant difference between groups. The reason for the greatest number of dead cells in the Moon group can be that had less cell medium concentration (15µl) and the area of the surface (2.4 mm) than other groups (3 mm). The area of live cells in the culture chamber was affected significantly by partial gravity as there was a significant difference between positive control (only effects of the magnetic field) and negative control. The live cells in Mars (n=3, **P=0.0041) and the Moon (n=3, **P=0.0095) groups were a reduction compared to the 1 g control groups (Figure 44-b), and the cells were affected by simulated partial gravity as being exposed to a new environment not experienced before. However, the analysis of the number of dead cells/areas of the live cells was no observed significant difference between groups.

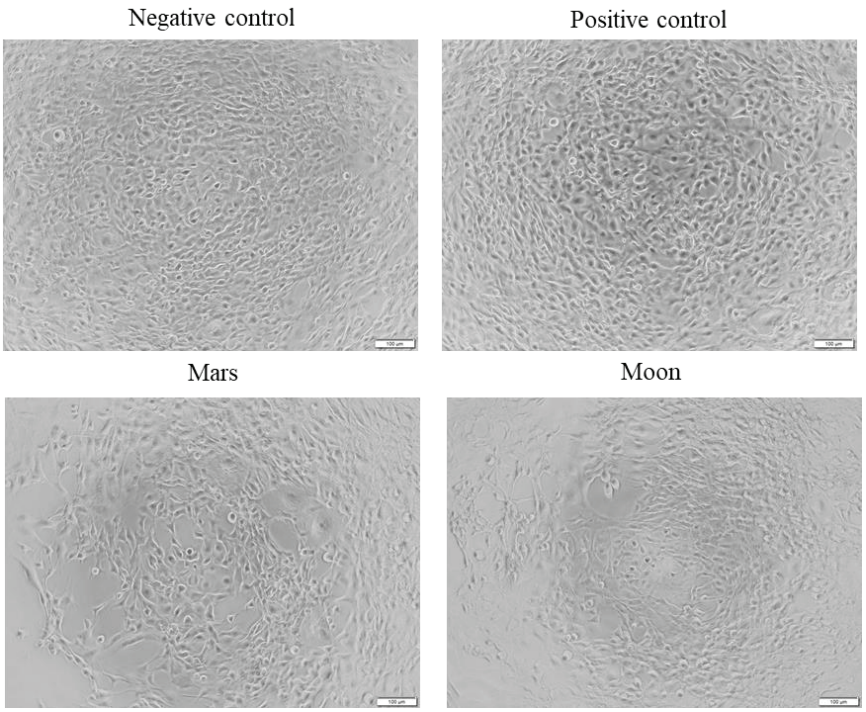

Figure 43. The phase images of the 7F2 cells exposed to simulated partial gravity for 24 h. Scale bar: 100 μm.

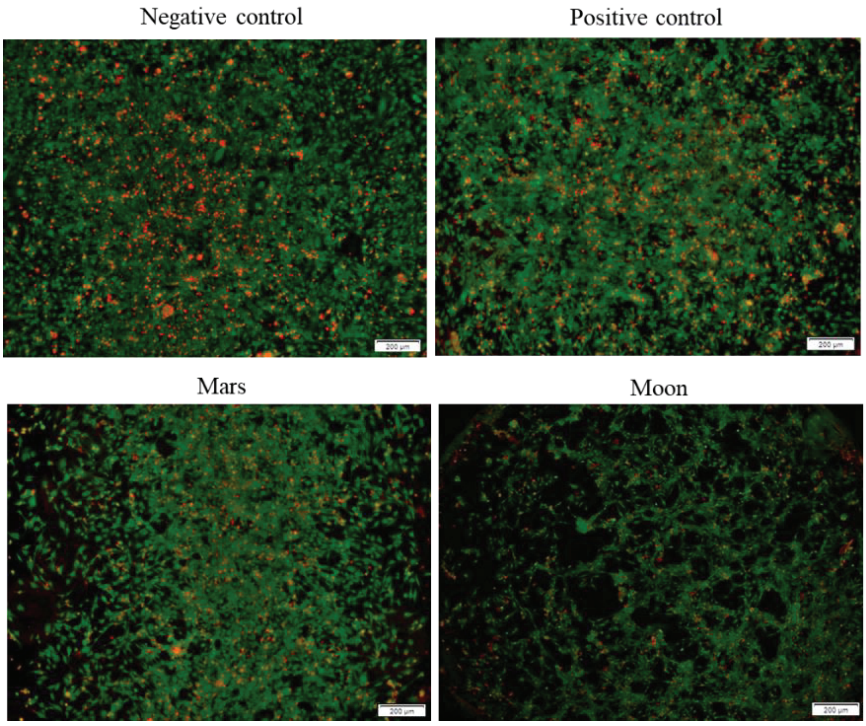

Figure 44. Representative images of cell viability was visualized by live-dead staining (Calcein/PI). Cells were cultured in the standard culture medium, as a

negative control and with exposure to a magnetic field of the magnets as a positive control and simulated partial gravity with 28 and 38 mM Gd^{3+} concentration for Mars and the Moon (live: green, dead: red). Scale bars: 200 µm.

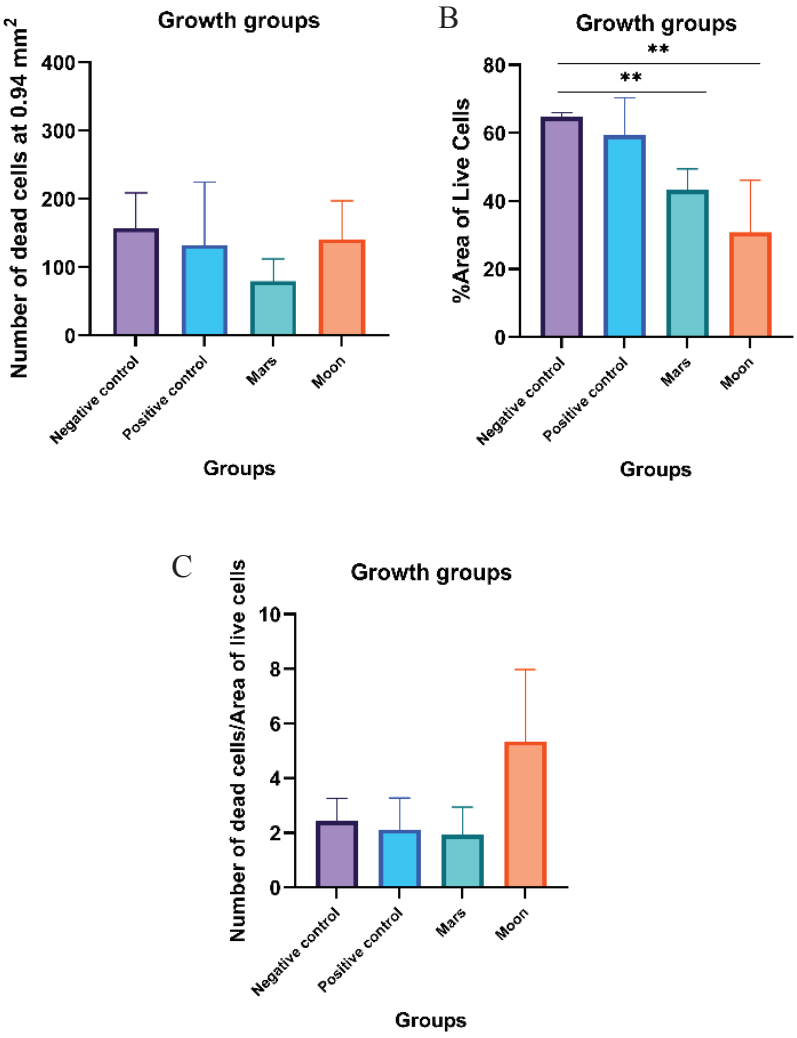

Figure 45. Cell viability was visualized by live-dead staining (Calcein/PI) and live and dead cells were quantitative value with ImageJ Fiji. A) The number of dead cells (red cells) at 0.94 mm^2. B) % Area of live cells (green area). Mars (n=3, **p < 0.01), Moon (n=3, **p < 0.01) with respect to control cells. C) The number of dead cells/ %Area of live cells. Statistical significance was assessed by un-paired t test (* p <0,05; ** p <0,01; *** p <0,005; **** p < 0,001). The error bars represent the standard deviation.

3.10. Determination of Effects of Simulated Partial Gravity on Cell Viability of Differentiated Osteoblast cells

To investigate the impact of partial gravity on osteogenic cells, 7F2 cells were induced osteogenesis with an osteogenic medium for 14 days. The mineralization was assessed with Alizarin Red S staining to visualize calcium deposits of a final step of differentiation of the osteoblasts at 14 days of the culture (Figure. 46). Following this, differentiated osteogenic cells were trypsinized and seeded at 15 x10^3/well concentrations in 25 µl with 28 mM Gd^{3+} into the Martian cell chamber and seeded at 15 x10^3/well in 15 µl with 38 mM Gd^{3+} into the Lunar cell chamber, and the cells were exposed to partial gravity for 24 hours.

After the exposure to partial gravity for 24 hours, it was taken phase images of the cells under the microscope to assess the attachment of the cells to the surface under partial gravity. The cells in positive and negative control groups showed the similar confluency of the cells, whereas the cells in Mars and the Moon groups had less confluency compared to the control groups (n=3). In order to investigate effects of simulated partial gravity on cell viability of osteogenic cells, the cell viability was determined with live/dead staining (Calcein-AM/PI). Osteogenic cells were affected by partial gravity; for this purpose, dead cells and the area of live cells were calculated with the ImageJ program. It was hard to analyze the number of live cells due to number of cells, therefore % area of live cells (green area) was analyzed with a basic ImageJ-based threshold extraction. The results showed the area of osteogenic cells in positive control, Mars and the Moon was less compared to the negative control. The osteogenic cells may be more sensitive against the magnetic field than undifferentiated 7F2 cells because there was a significant difference between negative and positive control. The area of live cells in positive control groups were exposed to only the magnetic field of the magnets without Gd^{3+}. However, especially the cells in Mars and the Moon groups showed significant differences compared to the negative control even if considering the influence of the magnetic field.

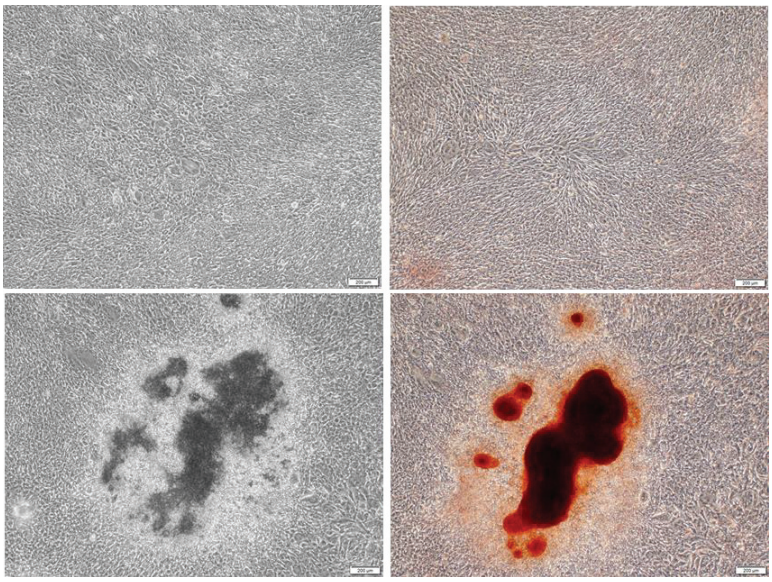

Figure 46. Images of calcium deposits of differentiated 7F2 cells with before and after Alizarin red staining at 14th days of culture. Scale bars: 200 μm.

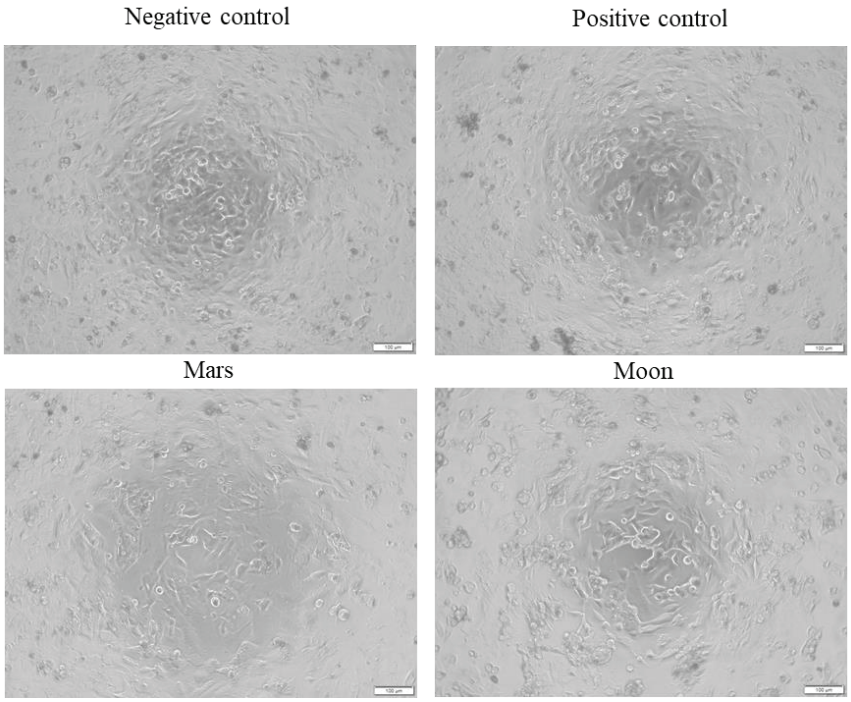

Figure 47. The phase images of the differentiated 7F2 cells exposed to simulated partial gravity for 24 h. Scale bar: 100 μm.

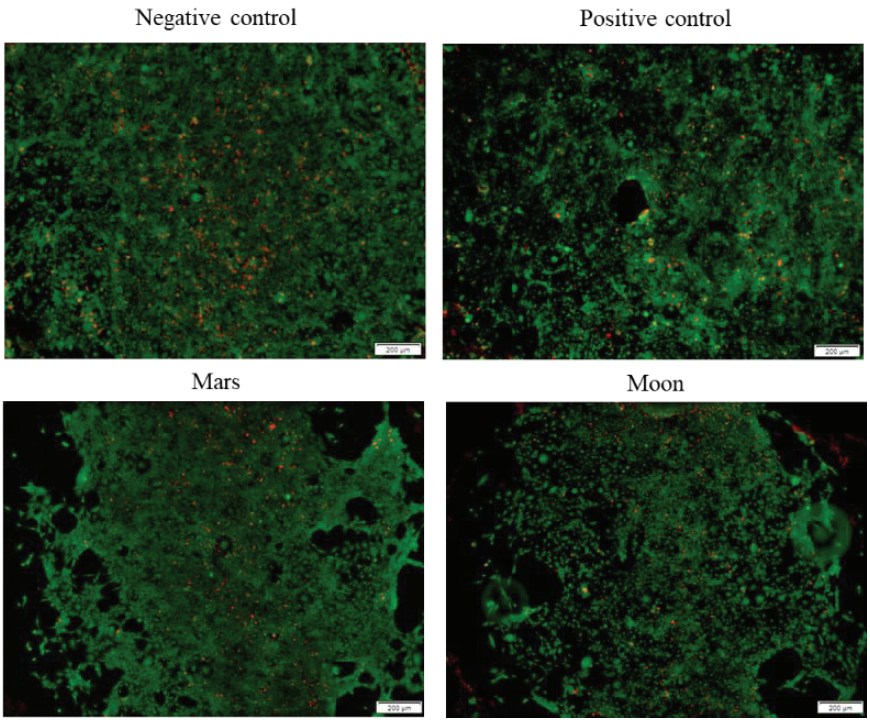

Figure 48. The representative images of cell viability was visualized by live-dead staining (Calcein/PI). Osteogenic cells were cultured in the osteogenic medium, as a negative control and with exposure to a magnetic field of the magnets as a positive control and simulated partial gravity with 28 and 38 mM Gd^{3+} concentration for Mars and the Moon (live: green, dead: red). Scale bars: 200 µm.

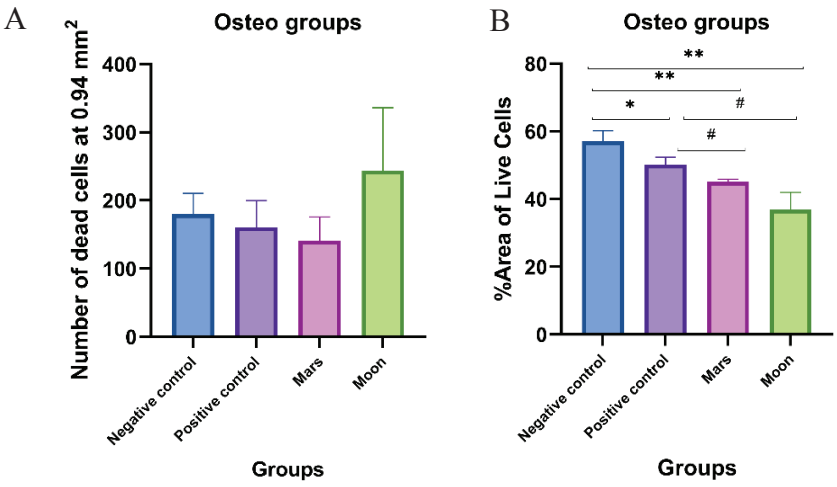

C

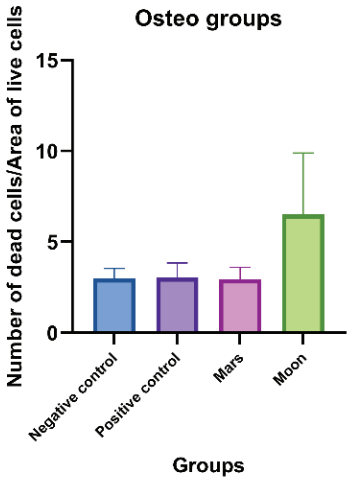

Figure 49. Cell viability was visualized by live-dead staining (Calcein/PI) and live and dead cells were quantitative value with ImageJ Fiji. A) The number of dead cells at 0.94 mm2. B) % Area of live cells (green area). Positive control (n=3, p= *0.0396), Mars (n=3, **p = 0.0035) and the Moon (n=3, **p= 0.0044) with respect to negative control cells. Mars (n=3, $^{\#}$p = 0.0171) the Moon (n=3, $^{\#}$p =0.0138) compared to positive control cells. C) Number of dead cells/%Area of live cells. Statistical significance was assessed by un-paired t test (* p< 0,05; ** p< 0,01; *** p< 0,005; **** p< 0,001). The error bars represent the standard deviation.

3.11. Examination of Effects of Simulated Partial Gravity on Cytoskeleton of Osteogenic cells

Next, to investigate effects of simulated partial gravity on cellular morphology of osteogenic cells, the cells were exposed to partial gravity for 24 h. Following 24 h, the F-actin filaments and nucleus were stained with phalloidin/dapi. According to the results, the simulated partial gravity did not lead to significant changes in F-actin filaments, but the number and length of filopodia-like structure in Mars, and the Moon cells was increased as a response partial gravity compared to negative control cells. However, the similar trend was observed in positive control. Therefore, this response may be related to magnetic field. For this, the intensity of stress fibers and the length and number of

filopodia of actins filaments should be more investigated to distinguish the effects of the partial gravity and magnetic field.

The MCF-7 cells exposed to real microgravity showed filopodia-like structures in F-actin filament [96]. A reduced number of stress fibers and abnormal actin cytoskeleton morphology in MC3T3-E1 osteoblasts was observed, also nuclei were oblong in shape and smaller than the ground controls [64].

In accordance with Figure 51, the nucleus circularity was quantified with ImageJ Fiji to examine whether simulated partial gravity effects on nucleus of the cells. The result showed simulated partial gravity strongly affected morphology of nucleus in osteogenic differentiated cells. Here it was shown that the magnetic field led to a decrease in cell circularity (0.816) compared to negative control. Partial gravity led to some changes in cellular morphology for 24 h cultured osteogenic differentiated cells. A significant increase was observed in the circularity of nuclei in Mars cells (0.850), while a significant decrease in the Moon (0.818) with respect to negative control (0.838). However, more studies are needed to confirm the effects of the simulated partial gravity on the nuclei.

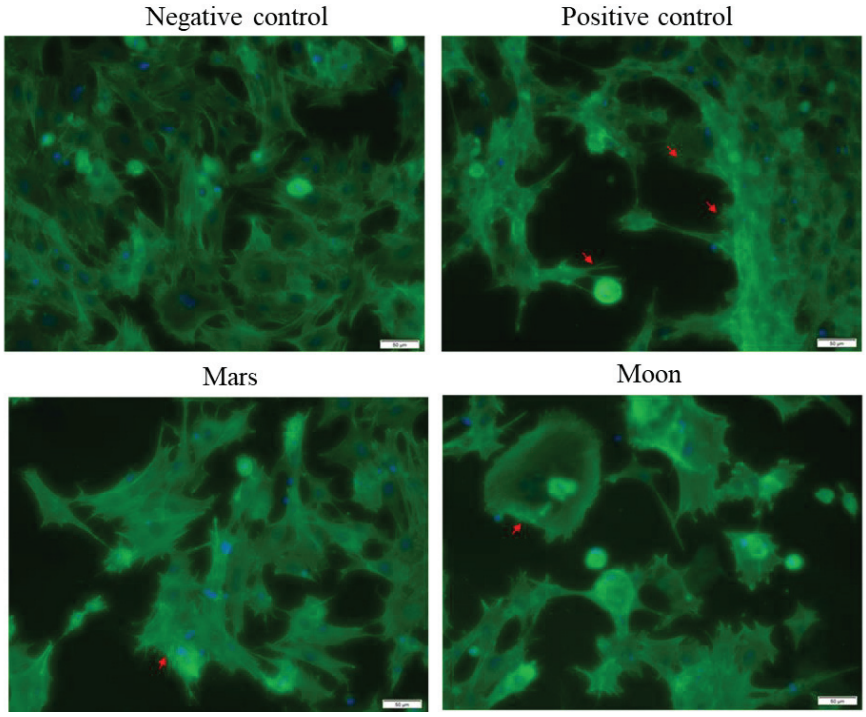

Figure 50. Representative images of the actin cytoskeleton staining with phalloidin/dapi. Actin filaments represented with green color and nuclei were represented with blue color. Scale bar: 50 μm.

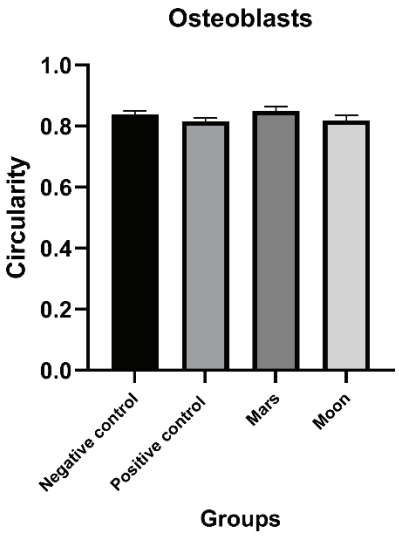

Figure 51. Circularity index of the nucleus for differentiated osteoblast cells exposure to the simulated partial gravity. The circularity of the nucleus was 0.850 on Mars, and 0.818 on the Moon, on the other hand, in negative control were 0.838, and 0.816 in positive control.

CHAPTER 4

CONCLUSION

It is crucial to understand the changes occurring in cells exposed to simulated partial gravity conditions because there are numerous unknowns regarding the changes that occur at the cellular and molecular level in response to partial gravity. In this present study, it was aimed to develop a new platform that is able to mimic the partial gravity of the Moon and Mars and to investigate the effects of partial gravity on the cellular level. First, reduced gravitational force was manipulated using Halbach array magnets and appropriate paramagnetic agent concentrations based on finite element method, and the partial gravity platform was designed according to the simulation results. The system was formed for the first time and conducted cellular level studies.

The effects of partial gravity on cell viability and morphology of 7F2 cells and osteogenic differentiated cells were observed exposed for 24 hours to simulated partial gravity (short-term). Simulated partial gravity led to a decreased area of live cells and a decline in the circularity size of the nucleus on the Moon, whereas an increase on Mars. However, the magnetic field caused a decrease in circularity in positive control. Therefore, the nuclei of the cells may be sensitive to the magnetic field. However, each ground-based simulation models are not perfect and have some limitations, such as shear stress.

Ground-based partial gravity models are valuable tools for the investigation of the effects of partial gravity. Our new platform may be a good alternative to examine the effects of partial gravity at the cellular level because this system is low-cost, allows short- and long-term cell culture studies, and can be used to development of potential countermeasures against the effects of partial gravity, contribute to therapeutics drug testing, but it should be investigated the effect of the magnetic field on cells extensively.

REFERENCES

1. Clément, G. *Fundamentals of Space Medicine*; 2005. https://doi.org/10.1007/1-4020-3434-2.

2. Clément, G. *Fundamentals of Space Medicine*; 2011. https://doi.org/10.1007/978-1-4419-9905-4.

3. Ozcivici, E.; Luu, Y. K.; Adler, B.; Qin, Y. X.; Rubin, J.; Judex, S.; Rubin, C. T. Mechanical Signals as Anabolic Agents in Bone. *Nature Reviews Rheumatology*. 2010. https://doi.org/10.1038/nrrheum.2009.239.

4. Özçivici, E. Effects of Spaceflight on Cells of Bone Marrow Origin. *Turkish Journal of Hematology* **2013**, *30* (1). https://doi.org/10.4274/tjh.2012.0127.

5. Ozcivici, E.; Zhang, W.; Donahue, L. R.; Judex, S. Quantitative Trait Loci That Modulate Trabecular Bone's Risk of Failure during Unloading and Reloading. *Bone* **2014**, *64*. https://doi.org/10.1016/j.bone.2014.03.042.

6. Judex, S.; Zhang, W.; Donahue, L. R.; Ozcivici, E. Genetic and Tissue Level Muscle-Bone Interactions during Unloading and Reambulation. *J Musculoskelet Neuronal Interact* **2016**, *16* (3), 174.

7. Vico, L.; Hargens, A. Skeletal Changes during and after Spaceflight. *Nature Reviews Rheumatology 2018 14:4* **2018**, *14* (4), 229–245. https://doi.org/10.1038/nrrheum.2018.37.

8. Hughson, R. L.; Shoemaker, J. K.; Blaber, A. P.; Arbeille, P.; Greaves, D. K.; Pereira-Junior, P. P.; Xu, D. Cardiovascular Regulation during Long-Duration Spaceflights to the International Space Station. *J Appl Physiol* **2012**, *112* (5). https://doi.org/10.1152/japplphysiol.01196.2011.

9. Shackelford, L. C. Musculoskeletal Response to Space Flight. In *Principles of Clinical Medicine for Space Flight*; 2020. https://doi.org/10.1007/978-1-4939-9889-0_19.

10. Sonnenfeld, G.; Shearer, W. T. Immune Function during Space Flight. *Nutrition* **2002**, *18* (10). https://doi.org/10.1016/S0899-9007(02)00903-6.

11. Borchers, A. T.; Keen, C. L.; Gershwin, M. E. Microgravity and Immune Responsiveness: Implications for Space Travel. *Nutrition* **2002**, *18* (10). https://doi.org/10.1016/S0899-9007(02)00913-9.

12. Boonyaratanakornkit, J. B.; Cogoli, † A; Li, C.-F.; Schopper, T.; Pippia, P.; Galleri, ‖ G; Meloni, M. A.; Hughes-Fulford, M.; Hughes-Fulford, M. Key Gravity-Sensitive Signaling Pathways Drive T-Cell Activation. *The FASEB Journal* **2005**. https://doi.org/10.1096/fj.05-3778fje.

13. Williams, D.; Kuipers, A.; Mukai, C.; Thirsk, R. Acclimation during Space Flight: Effects on Human Physiology. *CMAJ. Canadian Medical Association Journal*. 2009. https://doi.org/10.1503/cmaj.090628.

14. Norsk, P.; Asmar, A.; Damgaard, M.; Christensen, N. J. Fluid Shifts, Vasodilatation and Ambulatory Blood Pressure Reduction during Long Duration Spaceflight. *Journal of Physiology* **2015**, *593* (3). https://doi.org/10.1113/jphysiol.2014.284869.

15. Vico, L.; van Rietbergen, B.; Vilayphiou, N.; Linossier, M. T.; Locrelle, H.; Normand, M.; Zouch, M.; Gerbaix, M.; Bonnet, N.; Novikov, V.; Thomas, T.; Vassilieva, G. Cortical and Trabecular Bone Microstructure Did Not Recover at Weight-Bearing Skeletal Sites and Progressively Deteriorated at Non-Weight-Bearing Sites During the Year Following International Space Station Missions. *Journal of Bone and Mineral Research* **2017**, *32* (10). https://doi.org/10.1002/jbmr.3188.

16. Orwoll, E. S.; Adler, R. A.; Amin, S.; Binkley, N.; Lewiecki, E. M.; Petak, S. M.; Shapses, S. A.; Sinaki, M.; Watts, N. B.; Sibonga, J. D. Skeletal Health in Long-Duration Astronauts: Nature, Assessment, and Management Recommendations from the NASA Bone Summit. *Journal of Bone and Mineral Research*. 2013. https://doi.org/10.1002/jbmr.1948.

17. Vandenburgh, H.; Chromiak, J.; Shansky, J.; Tatto, M. del; Lemaire, J. Space Travel Directly Induces Skeletal Muscle Atrophy. *The FASEB Journal* **1999**, *13* (9), 1031–1038. https://doi.org/10.1096/FASEBJ.13.9.1031.

18. Vico, L.; Collet, P.; Guignandon, A.; Lafage-Proust, M. H.; Thomas, T.; Rehailia, M.; Alexandre, C. Effects of Long-Term Microgravity Exposure on Cancellous and Cortical Weight-Bearing Bones of Cosmonauts. *The Lancet* **2000**, *355* (9215), 1607–1611. https://doi.org/10.1016/S0140-6736(00)02217-0.

19. Smith, S. M.; Heer, M.; Shackelford, L. C.; Sibonga, J. D.; Spatz, J.; Pietrzyk, R. A.; Hudson, E. K.; Zwart, S. R. Bone Metabolism and Renal Stone Risk during International Space Station Missions. *Bone* **2015**, *81*, 712–720. https://doi.org/10.1016/J.BONE.2015.10.002.

20. NASA. NASA's Lunar Exploration Program Overview. *Nasa* **2020**, No. September.

21. Smith, M.; Craig, D.; Herrmann, N.; Mahoney, E.; Krezel, J.; McIntyre, N.; Goodliff, K. The Artemis Program: An Overview of NASA's Activities to Return Humans to the Moon. In *IEEE Aerospace Conference Proceedings*; 2020. https://doi.org/10.1109/AERO47225.2020.9172323.

22. Pletser, V.; Kumei, Y. Parabolic Flights. In *Generation and Applications of Extra-Terrestrial Environments on Earth*; 2015. https://doi.org/10.1201/9781003338277-9.

23. Shelhamer, M. Parabolic Flight as a Spaceflight Analog. *Journal of Applied Physiology*. 2016. https://doi.org/10.1152/japplphysiol.01046.2015.

24. Lotz, C.; Wessarges, Y.; Hermsdorf, J.; Ertmer, W.; Overmeyer, L. Novel Active Driven Drop Tower Facility for Microgravity Experiments Investigating Production Technologies on the Example of Substrate-Free Additive Manufacturing. *Advances in Space Research* **2018**, *61* (8), 1967–1974. https://doi.org/10.1016/J.ASR.2018.01.010.

25. Klaus, D. M. Clinostats and Bioreactors. *Gravit Space Biol Bull* **2001**, *14* (2).

26. Wuest, S. L.; Richard, S.; Kopp, S.; Grimm, D.; Egli, M. Simulated Microgravity: Critical Review on the Use of Random Positioning Machines for Mammalian Cell Culture. *Biomed Res Int* **2015**, *2015*. https://doi.org/10.1155/2015/971474.

27. Rucci, N.; Migliaccio, S.; Zani, B. M.; Taranta, A.; Teti, A. Characterization of the Osteoblast-like Cell Phenotype under Microgravity Conditions in the NASA-Approved Rotating Wall Vessel Bioreactor (RWV). *J Cell Biochem* **2002**, *85* (1). https://doi.org/10.1002/jcb.10120.

28. Anil-Inevi, M.; Sarigil, O.; Kizilkaya, M.; Mese, G.; Tekin, H. C.; Ozcivici, E. Stem Cell Culture under Simulated Microgravity. In *Advances in Experimental Medicine and Biology*; 2020; Vol. 1298. https://doi.org/10.1007/5584_2020_539.

29. Anil-Inevi, M.; Yaman, S.; Arslan Yildiz, A.; Mese, G.; Yalcin-Ozuysal, O.; Cumhur Tekin, H.; Ozcivici, E. Biofabrication of in Situ Self Assembled 3D Cell Cultures in a Weightlessness Environment Generated Using Magnetic Levitation OPEN. https://doi.org/10.1038/s41598-018-25718-9.

30. Herranz, R.; Larkin, O. J.; Dijkstra, C. E.; Hill, R. J. A.; Anthony, P.; Davey, M. R.; Eaves, L.; van Loon, J. J. W. A.; Medina, F. J.; Marco, R. Microgravity Simulation by Diamagnetic Levitation: Effects of a Strong Gradient Magnetic Field on the Transcriptional Profile of Drosophila Melanogaster. *BMC Genomics* **2012**, *13* (1). https://doi.org/10.1186/1471-2164-13-52.

31. Valles, J. M.; Maris, H. J.; Seidel, G. M.; Tang, J.; Yao, W. Magnetic Levitation-Based Martian and Lunar Gravity Simulator. In *Advances in Space Research*; 2005; Vol. 36. https://doi.org/10.1016/j.asr.2005.01.081.

32. Ritzmann, R.; Freyler, K.; Krause, A.; Gollhofer, A. Bouncing on Mars and the Moon-the Role of Gravity on Neuromuscular Control: Correlation of Muscle Activity and Rate of Force Development. *J Appl Physiol* **2016**, *121* (6). https://doi.org/10.1152/japplphysiol.00692.2016.

33. Benavides Damm, T.; Walther, I.; Wüest, S. L.; Sekler, J.; Egli, M. Cell Cultivation under Different Gravitational Loads Using a Novel Random Positioning Incubator. *Biotechnol Bioeng* **2014**, *111* (6). https://doi.org/10.1002/bit.25179.

34. Fengler, S.; Spirer, I.; Neef, M.; Ecke, M.; Hauslage, J.; Hampp, R. Changes in Gene Expression of Arabidopsis Thaliana Cell Cultures Upon Exposure to Real and Simulated Partial-g Forces. *Microgravity Sci Technol* **2016**, *28* (3). https://doi.org/10.1007/s12217-015-9452-y.

35. Mortreux, M.; Nagy, J. A.; Ko, F. C.; Bouxsein, M. L.; Rutkove, S. B. A Novel Partial Gravity Ground-Based Analog for Rats via Quadrupedal Unloading. *J Appl Physiol* **2018**, *125* (1). https://doi.org/10.1152/japplphysiol.01083.2017.

36. Mortreux, M.; Riveros, D.; Bouxsein, M. L.; Rutkove, S. B. Mimicking a Space Mission to Mars Using Hindlimb Unloading and Partial Weight Bearing in Rats. *Journal of Visualized Experiments* **2019**, *2019* (146). https://doi.org/10.3791/59327.

37. Cutuk, A.; Groppo, E. R.; Quigley, E. J.; White, K. W.; Pedowitz, R. A.; Hargens, A. R. Ambulation in Simulated Fractional Gravity Using Lower Body Positive Pressure: Cardiovascular Safety and Gait Analyses. *J Appl Physiol* **2006**, *101* (3). https://doi.org/10.1152/japplphysiol.00644.2005.

38. Kram, R.; Domingo, A.; Ferris, D. P. Effect of Reduced Gravity on the Preferred Walk-Run Transition Speed. *J Exp Biol* **1997**, *200* (Pt 4), 821–826. https://doi.org/10.1242/JEB.200.4.821.

39. Sylos-Labini, F.; Ivanenko, Y. P.; Cappellini, G.; Portone, A.; Maclellan, M. J.; Lacquaniti, F. Changes of Gait Kinematics in Different Simulators of Reduced Gravity. *J Mot Behav* **2013**, *45* (6). https://doi.org/10.1080/00222895.2013.833080.

40. Katayama, K.; Sato, K.; Akima, H.; Ishida, K.; Takada, H.; Watanabe, Y.; Iwase, M.; Miyamura, M.; Iwase, S. Acceleration with Exercise during Head-down Bed Rest Preserves Upright Exercise Responses. *Aviat Space Environ Med* **2004**, *75* (12).

41. Cavanagh, P. R.; Rice, A. J.; Licata, A. A.; Kuklis, M. M.; Novotny, S. C.; Genc, K. O.; Englehaupt, R. K.; Hanson, A. M. A Novel Lunar Bed Rest Analogue. *Aviat Space Environ Med* **2013**, *84* (11). https://doi.org/10.3357/ASEM.3472.2013.

42. Pletser, V. Short Duration Microgravity Experiments in Physical and Life Sciences during Parabolic Flights: The First 30 ESA Campaigns. *Acta Astronaut* **2004**, *55* (10), 829–854. https://doi.org/10.1016/J.ACTAASTRO.2004.04.006.

43. Mortreux, M.; Rosa-Caldwell, M. E. Approaching Gravity as a Continuum Using the Rat Partial Weight-Bearing Model. *Life*. 2020. https://doi.org/10.3390/life10100235.

44. Semple, C.; Riveros, D.; Nagy, J. A.; Rutkove, S. B.; Mortreux, M. Partial Weight-Bearing in Female Rats: Proof of Concept in a Martian-Gravity Analog. *Front Physiol* **2020**, *11*. https://doi.org/10.3389/fphys.2020.00302.

45. Zhang, S.; Ueno, D.; Ohira, T.; Kato, H.; Izawa, T.; Yamanouchi, S.; Yoshida, Y.; Takahashi, A.; Ohira, Y. Depression of Bone Density at the Weight-Bearing Joints in Wistar Hannover Rats by a Simulated Mechanical Stress Associated With Partial Gravity Environment. *Front Cell Dev Biol* **2021**, *9*. https://doi.org/10.3389/fcell.2021.707470.

46. Takahashi, A.; Yamanouchi, S.; Takeuchi, K.; Takahashi, S.; Tashiro, M.; Hidema, J.; Higashitani, A.; Adachi, T.; Zhang, S.; Guirguis, F. N. L.; Yoshida, Y.; Nagamatsu, A.; Hada, M.; Takeuchi, K.; Takahashi, T.; Sekitomi, Y. Combined Environment Simulator for Low-Dose-Rate Radiation and Partial Gravity of Moon and Mars. *Life* **2020**, *10* (11). https://doi.org/10.3390/life10110274.

47. Wuest, S. L.; Richard, S.; Kopp, S.; Grimm, D.; Egli, M. Simulated Microgravity: Critical Review on the Use of Random Positioning Machines for Mammalian Cell Culture. *Biomed Res Int* **2015**, *2015*. https://doi.org/10.1155/2015/971474.

48. Ferranti, F.; Bianco, M. del; Pacelli, C. Advantages and Limitations of Current Microgravity Platforms for Space Biology Research. **2020**. https://doi.org/10.3390/app11010068.

49. Ritzmann, R.; Freyler, K.; Krause, A.; Gollhofer, A.; Bouncing, G. A. Bouncing on Mars and the Moon-the Role of Gravity on Neuromuscular Control: Correlation of Muscle Activity and Rate of Force Development. *J Appl Physiol* **2016**, *121*, 1187–1195. https://doi.org/10.1152/japplphysiol.00692.2016.-On.

50. Raggatt, L. J.; Partridge, N. C. Cellular and Molecular Mechanisms of Bone Remodeling. *Journal of Biological Chemistry* **2010**, *285* (33), 25103–25108. https://doi.org/10.1074/JBC.R109.041087.

51. Florencio-Silva, R.; Sasso, G. R. D. S.; Sasso-Cerri, E.; Simões, M. J.; Cerri, P. S. Biology of Bone Tissue: Structure, Function, and Factors That Influence Bone Cells. *Biomed Res Int* **2015**, *2015*. https://doi.org/10.1155/2015/421746.

52. Kostenuik, P. J.; Halloran, B. P.; Morey-Holton, E. R.; Bikle, D. D. Skeletal Unloading Inhibits the in Vitro Proliferation and Differentiation of Rat Osteoprogenitor Cells. American Journal *of* Physiology-Endocrinology and Metabolism*,* **1997**, *273* (6 36-6). https://doi.org/10.1152/ajpendo.1997.273.6.e1133.

53. Rachner, T. D.; Khosla, S.; Hofbauer, L. C. Osteoporosis: Now and the Future. *The Lancet*. 2011. https://doi.org/10.1016/S0140-6736(10)62349-5.

54. Seeman, E. Reduced Bone Formation and Increased Bone Resorption: Rational Targets for the Treatment of Osteoporosis. *Osteoporos Int* **2003**, *14 Suppl 3*. https://doi.org/10.1007/S00198-002-1340-9.

55. Baskan, O.; Karadas, O.; Mese, G.; Ozcivici, E. Applicability of Low-Intensity Vibrations as a Regulatory Factor on Stem and Progenitor Cell Populations. *Curr Stem Cell Res Ther* **2019**, *15* (5). https://doi.org/10.2174/1574888x14666191212155647.

56. Olçum, M.; Baskan, Ö.; Karadaş, Ö.; Özçivici, E. Application of Low Intensity Mechanical Vibrations for Bone Tissue Maintenance and Regeneration. *Turkish Journal of Biology*. 2016. https://doi.org/10.3906/biy-1506-76.

57. Tamma, R.; Colaianni, G.; Camerino, C.; Benedetto, A. di; Greco, G.; Strippoli, M.; Vergari, R.; Grano, A.; Mancini, L.; Mori, G.; Colucci, S.; Grano, M.; Zallone, A. Microgravity during Spaceflight Directly Affects in Vitro Osteoclastogenesis and Bone Resorption. *The FASEB Journal* **2009**, *23* (8), 2549–2554. https://doi.org/10.1096/FJ.08-127951.

58. Chau, J. F. L.; Leong, W. F.; Li, B. Signaling Pathways Governing Osteoblast Proliferation, Differentiation and Function. *Histology and Histopathology*. 2009. https://doi.org/10.14670/HH-24.1593.

59. Krause, U.; Seckinger, A.; Gregory, C. A. Assays of Osteogenic Differentiation by Cultured Human Mesenchymal Stem Cells. *Methods Mol Biol* **2011**, *698*. https://doi.org/10.1007/978-1-60761-999-4_17.

60. Truesdell, S. L.; Saunders, M. M. Bone Remodeling Platforms: Understanding the Need for Multicellular Lab-on-a-Chip Systems and Predictive Agent-Based Models. *Mathematical Biosciences and Engineering* **2020**, *17* (2). https://doi.org/10.3934/mbe.2020063.

61. Hughes-Fulford, M. The Role of Signaling Pathways in Osteoblast Gravity Perception. In *European Space Agency, (Special Publication) ESA SP*; 2002.

62. Buravkova, L. B.; Gershovich, P. M.; Gershovich, J. G.; Grigorev, A. I. Mechanisms of Gravitational Sensitivity of Osteogenic Precursor Cells. *Acta Naturae* **2010**, *2* (1). https://doi.org/10.32607/actanaturae.10734.

63. Nabavi, N.; Khandani, A.; Camirand, A.; Harrison, R. E. Effects of Microgravity on Osteoclast Bone Resorption and Osteoblast Cytoskeletal Organization and Adhesion. *Bone* **2011**, *49* (5). https://doi.org/10.1016/j.bone.2011.07.036.

64. Hughes-Fulford, M.; Lewis, M. L. Effects of Microgravity on Osteoblast Growth Activation. *Exp Cell Res* **1996**, *224* (1). https://doi.org/10.1006/excr.1996.0116.

65. Zayzafoon, M.; Gathings, W. E.; McDonald, J. M. Modeled Microgravity Inhibits Osteogenic Differentiation of Human Mesenchymal Stem Cells and Increases Adipogenesis. *Endocrinology* **2004**, *145* (5). https://doi.org/10.1210/en.2003-1156.

66. Braveboy-Wagner, J.; Lelkes, P. I. ARTICLE Impairment of 7F2 Osteoblast Function by Simulated Partial Gravity in a Random Positioning Machine. https://doi.org/10.1038/s41526-022-00202-x.

67. Hughes-Fulford, M. Function of the Cytoskeleton in Gravisensing during Spaceflight. *Advances in Space Research* **2003**, *32* (8). https://doi.org/10.1016/S0273-1177(03)90399-1.

68. Dai, Z.; Tan, Y.; Yang, F.; Qu, L.; Zhang, H.; Wan, Y.; Li, Y. Altered Actin Dynamics and Functions of Osteoblast-like Cells in Parabolic Flight May Involve ERK1/2. *Microgravity Sci Technol* **2011**, *23* (1). https://doi.org/10.1007/s12217-010-9216-7.

69. Schön, S. J. *Chapter 10 - Magnetic Properties*; 2011; Vol. 8.

70. Spain, E.; Venkatanarayanan, A. Review of Physical Principles of Sensing and Types of Sensing Materials. In *Comprehensive Materials Processing*; 2014; Vol. 13. https://doi.org/10.1016/B978-0-08-096532-1.01302-9.

71. Fox, A. M. Magnetism and Magnetic Materials, by J.M.D. Coey. *Contemp Phys* **2011**, *52* (1). https://doi.org/10.1080/00107514.2010.514061.

72. Pardasani, R. T.; Pardasani, P. *Magnetic Properties of Paramagnetic Compounds, Magnetic Susceptibility Data, Volume 3*; 2021. https://doi.org/10.1007/978-3-662-62470-8.

73. Blums, E.; Cebers, A.; Maiorov, M. M. *Magnetic Fluids*; 2010. https://doi.org/10.3367/ufnr.0112.197403b.0427.

74. Jiles, D. *Introduction to Magnetism and Magnetic Materials*; 2015. https://doi.org/10.1201/b18948.

75. Sherry, A. D.; Caravan, P.; Lenkinski, R. E. Primer on Gadolinium Chemistry. In *Journal of Magnetic Resonance Imaging*; 2009; Vol. 30. https://doi.org/10.1002/jmri.21966.

76. Rogosnitzky, M.; Branch, S. Gadolinium-Based Contrast Agent Toxicity: A Review of Known and Proposed Mechanisms. *Biometals* **2016**, *29* (3), 365–376. https://doi.org/10.1007/S10534-016-9931-7.

77. H, S.-W. Stability of Linear and Macrocyclic Gadolinium Based Contrast Agents. *Br J Radiol* **2007**, *80* (955), 581–582. https://doi.org/10.1259/BJR/17326033.

78. Sarigil, O.; Anil-Inevi, M.; Yilmaz, E.; Mese, G.; Tekin, H. C.; Ozcivici, E. Label-Free Density-Based Detection of Adipocytes of Bone Marrow Origin Using Magnetic Levitation. *Analyst* **2019**, *144* (9). https://doi.org/10.1039/c8an02503g.

79. Sarigil, O.; Anil-Inevi, M.; Firatligil-Yildirir, B.; Unal, Y. C.; Yalcin-Ozuysal, O.; Mese, G.; Tekin, H. C.; Ozcivici, E. Scaffold-Free Biofabrication of Adipocyte Structures with Magnetic Levitation. *Biotechnol Bioeng* **2021**, *118* (3). https://doi.org/10.1002/bit.27631.

80. Delikoyun, K.; Yaman, S.; Yilmaz, E.; Sarigil, O.; Anil-Inevi, M.; Telli, K.; Yalcin-Ozuysal, O.; Ozcivici, E.; Tekin, H. C. HologLev: A Hybrid Magnetic Levitation Platform Integrated with Lensless Holographic Microscopy for Density-Based Cell Analysis. *ACS Sens* **2021**, *6* (6). https://doi.org/10.1021/acssensors.0c02587.

81. Anil-Inevi, M.; Delikoyun, K.; Mese, G.; Tekin, H. C.; Ozcivici, E. Magnetic Levitation Assisted Biofabrication, Culture, and Manipulation of 3D Cellular Structures Using a Ring Magnet Based Setup. *Biotechnol Bioeng* **2021**, *118* (12). https://doi.org/10.1002/bit.27941.

82. Baskan, O.; Sarigil, · Oyku; Mese, G.; Ozcivici, · Engin. Frequency-Specific Sensitivity of 3T3-L1 Preadipocytes to Low-Intensity Vibratory Stimulus during Adipogenesis. *In Vitro Cell Dev Biol Anim* **2022**. https://doi.org/10.1007/s11626-022-00696-5.

83. Trog, S.; El-Khatib, A. H.; Beck, S.; Makowski, M. R.; Jakubowski, N.; Linscheid, M. W. Complementarity of Molecular and Elemental Mass Spectrometric Imaging of Gadovist ™ in Mouse Tissues. *Anal Bioanal Chem* **2019**, *411* (3), 629–637. https://doi.org/10.1007/S00216-018-1477-9/FIGURES/5.

84. Hilton, J. E.; McMurry, S. M. An Adjustable Linear Halbach Array. *Journal of Magnetism and Magnetic Materials,* **2012**, *324* (13), 2051–2056. https://doi.org/10.1016/J.JMMM.2012.02.014.

85. Boisclair, J.; Richard, P. L.; Laliberté, T.; Gosselin, C. Gravity Compensation of Robotic Manipulators Using Cylindrical Halbach Arrays. *IEEE/ASME Transactions on Mechatronics* **2017**, *22* (1), 457–464. https://doi.org/10.1109/TMECH.2016.2614386.

86. Raich, H.; Blu¨mler, P.; Blu¨mler, B. Design and Construction of a Dipolar Halbach Array with a Homogeneous Field from Identical Bar Magnets: NMR Mandhalas. **2004**. https://doi.org/10.1002/cmr.b.20018.

87. Saeed, O.; Duru, I.; Yulin, D. Magnetic Microfluidic Linear Halbach Array Configuration for Cell Separation. In *MATEC Web of Conferences*; 2018; Vol. 153. https://doi.org/10.1051/matecconf/201815306008.

88. Hoyos, M.; Moore, L.; Williams, P. S.; Zborowski, M. The Use of a Linear Halbach Array Combined with a Step-SPLITT Channel for Continuous Sorting of Magnetic Species. In *Journal of Magnetism and Magnetic Materials*; 2011; Vol. 323. https://doi.org/10.1016/j.jmmm.2010.11.051.

89. Kang, J. H.; Driscoll, H.; Super, M.; Ingber, D. E. Application of a Halbach Magnetic Array for Long-Range Cell and Particle Separations in Biological Samples. *Appl Phys Lett* **2016**, *108* (21). https://doi.org/10.1063/1.4952612.

90. Demiray, L.; Özçivici, E. Bone Marrow Stem Cells Adapt to Low-Magnitude Vibrations by Altering Their Cytoskeleton during Quiescence and Osteogenesis. *Turkish Journal of Biology* **2015**, *39* (1). https://doi.org/10.3906/biy-1404-35.

91. Baskan, O.; Mese, G.; Ozcivici, E. Low-Intensity Vibrations Normalize Adipogenesis-Induced Morphological and Molecular Changes of Adult Mesenchymal Stem Cells. *Proc Inst Mech Eng H* **2017**, *231* (2). https://doi.org/10.1177/0954411916687338.

92. Anil-Inevi, M.; Unal, Y. C.; Yaman, S.; Tekin, H. C.; Mese, G.; Ozcivici, E. Assessment of Cell Cycle and Viability of Magnetic Levitation Assembled Cellular Structures. In *TIPTEKNO 2020 - Tip Teknolojileri Kongresi - 2020 Medical Technologies Congress, TIPTEKNO 2020*; 2020. https://doi.org/10.1109/TIPTEKNO50054.2020.9299216.

93. Türker, E.; Demirçak, N.; Arslan-Yildiz, A. Scaffold-Free Three-Dimensional Cell Culturing Using Magnetic Levitation. *Biomater Sci* **2018**, *6* (7). https://doi.org/10.1039/c8bm00122g.

94. Durmus, N. G.; Tekin, H. C.; Guven, S.; Sridhar, K.; Yildiz, A. A.; Calibasi, G.; Ghiran, I.; Davis, R. W.; Steinmetz, L. M.; Demirci, U. Magnetic Levitation of Single Cells. *Proc Natl Acad Sci U S A* **2015**, *112* (28). https://doi.org/10.1073/pnas.1509250112.

95. Tocchio, A.; Durmus, N. G.; Sridhar, K.; Mani, V.; Coskun, B.; el Assal, R.; Demirci, U. Magnetically Guided Self-Assembly and Coding of 3D Living Architectures. *Advanced Materials* **2018**, *30* (4). https://doi.org/10.1002/adma.201705034.

96. Nassef, M. Z.; Kopp, S.; Wehland, M.; Melnik, D.; Sahana, J.; Krüger, M.; Corydon, T. J.; Oltmann, H.; Schmitz, B.; Schütte, A.; Bauer, T. J.; Infanger, M.; Grimm, D. Real Microgravity Influences the Cytoskeleton and Focal Adhesions in Human Breast Cancer Cells. *Int J Mol Sci* **2019**, *20* (13). https://doi.org/10.3390/ijms20133156.